Original Article

Impact of Cerium Oxide Nanoparticles versus Quercetin on Doxorubicin Induced Nephropathy in Adult Male Rats: Biochemical, Histological and Immunohistochemical Study

Sherine Ahmed Mohammed, Doha Saber Mohamed, Asmahan Sabry khalifa and Samira Mahmoud Mohamed

Department of Histology, Faculty of Medicine, Sohag University, Egypt

ABSTRACT

Introduction: Doxorubicin (DOX) induced nephropathy is a commonly used model. Cerium oxide nanoparticles (CeO2NPs) have anti-inflammatory and antioxidant roles. Quercetin is a polyphenolic structure found in different plant products and acts as an antioxidant.

Objective: The current study was conducted to compare the possible therapeutic effect of CeO2NPs versus quercetin against DOX-induced nephropathy at different time points.

Material and Methods: Fifty- five rats were divided into five groups. Control group (group I). Induction of nephropathy: rats were intraperitoneally injected with DOX in a dose of 2.5 mg/Kg BW day after day for 2 weeks then: Group II (DOX-treated groups): rats were sacrificed after 3 weeks of cessation of DOX injection in group IIa and 5 weeks of cessation of DOX injection in group IIb. Group III (DOX + CeO2NPs group): received CeO2 NPs for two weeks following 3 weeks of cessation of DOX injection in group IIIa and 5 weeks of cessation of DOX injection in group IIIb. Group IV (DOX + quercetin group): received quercetin for two weeks following 3 weeks of cessation of DOX injection in group IIIa and 5 weeks of cessation of DOX injection in group IIIb. Group V: cessation of DOX injection for 7 weeks. Biochemical, light microscopic, and ultrastructural studies were done. PCNA and WT-1 count and AFP immunohistochemical expression were measured.

Results: DOX-treated groups exhibited increased serum urea and creatinine, widened Bowman's space, degenerative changes in renal tubules, and increased collagen fibers which were more prominent in group IIb. Ultrastructurally, effacement of podocytes was seen. Significantly decreased WT-1 expression and increased PCNA and AFP were detected. CeO2NPs were more effective compared to quercetin in attenuating renal degenerative changes in DOX-induced nephropathy.

Conclusion: DOX caused duration-dependent renal toxicity. CeO2NPs were more effective than quercetin in attenuating renal degenerative changes in DOX-induced nephropathy.

Received: 23 December 2022, **Accepted:** 04 January 2023

Key Words: CeO2 NPs, dox induced nephropathy, quercetin, WT-1.

Corresponding Author: Sherine Ahmed Mohammed, MD, Department of Histology, Faculty of Medicine, Sohag University, Sohag, Egypt, **Tel.**: +20 11 2030 1020, **E-mail:** loua.sherine@ yahoo.com

ISSN: 1110-0559, Vol. 47, No. 1

INTRODUCTION

Doxorubicin (DOX) is a common chemotherapeutic drug that is used for treating different types of cancer[1]. However, DOX has toxic effects on different organs including the kidney[2]. DOX-induced model of nephropathy was commonly used in previous studies[3]. DOX induces nephropathy via different mechanisms including oxidative stress, inflammation as well as direct damage to the filtration barrier[4].

Nanotechnology is an emerging field of science. Cerium is a lanthanide metal that has two forms of oxide[5]. It was successfully converted into nanoparticles. Cerium oxide nanoparticles (CeO2NPs) have many medical applications, due to their small size and high surface-to-volume ratio. They have anti-inflammatory, antioxidant as well as anti-apoptotic properties[6]. They could improve tubular degeneration in thioacetamide-induced renal injury[7] and attenuate diabetic nephropathy[8]. In addition, Oró *et al*.[9] reported an antifibrotic effect of CeO2NPs in a rat model of hepatic fibrosis.

Quercetin is a type of polyphenolic structure found in different plant products. Its anti-oxidant, antiproliferative as well as anti-inflammatory activities were reported[10]. Quercetin improved kidney function and structure in a previously induced chronic renal disease model[11]. Quercetin attenuated cadmium chloride-induced renal injury in rats through suppression of endoplasmic reticulum stress[12]. This study aimed to compare the possible ameliorative effect of CeO2NPs versus quercetin against the DOX-induced model of nephropathy.

MATERIAL AND METHODS

Animals

Fifty-five adult male albino rats; 8-12 weeks old and 200-250 gm average weight, were used. Rats were kept at Sohag Experimental Animal Facility, Sohag University

 DOI: 10.21608/ejh.2023.181409.1834

with free access to water and food. They were acclimatized for 5 days prior to the experiment. All experimental procedures were approved by the Ethical Committee of the Faculty of Medicine, Sohag University with code: IRB00013006 Sohag IACUC 5 11 2022 6.

Chemicals

i. DOX was obtained from Sigma Aldrich Company (Adricin, Sigma Aldrich, St. Louis, Missouri, USA) and was freshly prepared by dissolving in saline; a 50 mg vial of DOX is dissolved in 25 ml saline to give 1.25 ml/kg.

ii. CeO2NPs (10 nm particle size) were obtained from Sigma-Aldrich® (St Louis, MO, USA).

iii. Quercetin was bought from Thermo Scientific Company, Neomarks, Fremont, USA.

iv. Antibodies:

A. Mouse monoclonal proliferating cell nuclear antigen (PCNA) antibody (PC10) (In*vitro*gen, Neomarks, Fremont, USA, Catalog # 13-3900).

B. Rabbit polyclonal Alpha-FetoProtein (AFP) (Thermo scientific company, Neomarks, Fremont, USA, Cat. #RB-9064-P0).

C. Rabbit monoclonal Wilms tumor-1 (WT-1) antibody (Abclonal, Woburn, Cat. #A2446)

Methods

Experimental design

55 animals were used, and divided into five groups:

Group I: The control group was subdivided into three subgroups:

- Subgroup Ia: 5 animals were intraperitoneally injected with saline and 5 animals received oral saline for 2 weeks after 5 weeks of saline intraperitoneal injection.
- Subgroup Ib: 5 animals were intraperitoneally injected with CeO2NPs in a dose of 0.5 m/kg body weight (BW) once per week for 2 weeks[13] after 5 weeks of saline intraperitoneal injection.
- Subgroup Ic: 5 animals received oral quercetin in a dose of 50 mg/kg BW once daily for two weeks[14] after 5 weeks of saline intraperitoneal injection.

Group II (DOX-treated groups):

- Group IIa:5 rats were intraperitoneally injected with DOX in a dose of 2.5 mg/Kg BW day after day for 2 weeks[15] and then injected with saline for the following 3 weeks.
- Group IIb:5rats were intraperitoneally injected with DOX in a dose of 2.5 mg/Kg BW day after day for 2 weeks[15] then injected with saline for the following 5 weeks.

Group III (DOX + CeO2NPs group):

- Group IIIa: 5 rats were intraperitoneally injected with DOX in a dose of 2.5 mg/Kg BW day after day for 2 weeks[15] and then injected with saline for the following 3 weeks. After that, they were intraperitoneally injected with CeO2NPs (0.5mg/kg BW) once per week for the subsequent 2 weeks[13].
- Group IIIb: 5 rats were intraperitoneally injected with DOX in a dose of 2.5 mg/Kg BW day after day for 2 weeks[15] then injection injected with saline for the following 5 weeks. After that, they were intraperitoneally injected with CeO2NPs (0.5mg /kg BW) once per week for the subsequent 2 weeks[13].

Group IV (DOX + quercetin group):

- Group IVa: 5 rats were intraperitoneally injected with DOX in a dose of 2.5 mg/Kg day after day for 2 weeks[15] and then injected with saline for the following 3 weeks. After that, they were given oral quercetin (50 mg/kg BW) once daily for the subsequent 2 weeks[14].
- Group IVb: 5 rats were intraperitoneally injected with DOX in a dose of 2.5 mg/Kg BW day after day for 2 weeks[15] and then injected with saline for the following 5 weeks. After that, they were given oral quercetin (50 mg/kg BW) once daily for the subsequent 2 weeks[14].

Group V: 5 rats were intraperitoneally injected with DOX in a dose of 2.5 mg/Kg BW day after day for 2 weeks[16] and then injected with saline for the following 7 weeks.

The study design is summarized in (Figure 1)

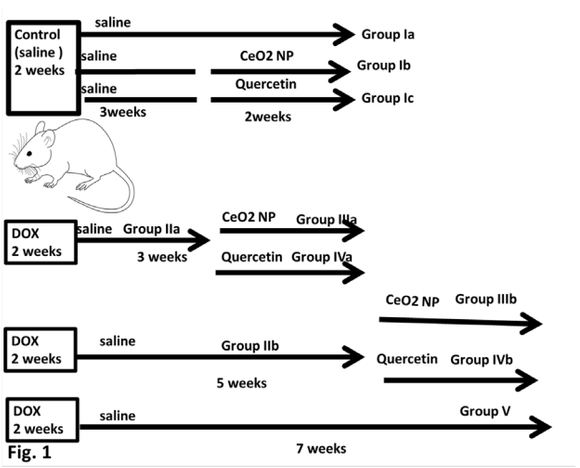

Fig. 1: Graphic presentation of the experimental design. CeO2NP: cerium oxide nanoparticles. DOX: doxorubicin.

At the end of the experiment, animals fasted overnight. They were anesthetized by inhalation of diethyl ether and

each animal was weighed. Blood samples were obtained by cardiac puncture and collected into non-heparinized tubes and were then centrifuged at 3000 r/min for 10 min for biochemical studies.

Animal body weight and relative kidney weight

Body weight was recorded for each animal. After the dissection, the right kidney was weighed and relative kidney weight was calculated in each animal as kidney weight in mg/ body weight in gm[17].

Biochemical studies

The following biochemical parameters were measured:

1. Serum urea and creatinine: Colorimetric Assay kits[18,19]
2. Serum albumin: commercial kits
3. Lipid profile:

Serum triglycerides, total cholesterol, and high-density lipoproteins (HDL) were measured by spectrophotometry using commercial kits (Human Gesellschaft fur Biochemica and Diagnostic, ambH, Wiesbaden, Germany) according to manufacturer instructions.

Histological and immunohistochemical studies

Kidney specimens were processed for light and electron microscopic studies and immunohistochemical staining.

A. Light microscopy

Right kidneys from all animals were cut into small pieces and were immediately fixed in a 10% neutral buffered formalin. Dehydration was done in ascending grades of ethyl alcohol. Clearing in xylene, and then embedding in paraffin were done. Blocks were sliced into thin sections (5µm in thickness) by microtome and mounted on glass slides. The mounted tissue was stained by the following stains:

1. Hematoxylin and eosin (H&E) for general histological studies.
2. Periodic acid Schiff (PAS) stain for demonstration of basement membranes and brush borders.
3. Masson trichrome stain for demonstration of collagen fibers.

The previous staining methods were applied according to Bancroft and Layton[20]

B. Immunohistochemical studies

PCNA antibody was used to detect cell proliferation(1:200 dilution), WT-1 antibody was used for identifying normal podocytes (1:100 dilution), and AFP was used to detect inflammation(1:100 dilution). Deparaffinization in xylene and rehydration of sections were done. Antigen retrieval was carried out in citrate buffer solution (PH 6.0) boiling in the microwave. The endogenous peroxidase was blocked by 0.3% hydrogen peroxide for 5 min. Incubation of the sections was done overnight at 4ºC with the primary antibody then the avidin-biotin technique was used. Sections were counterstained with Mayer's Hematoxylin, dehydrated, and cleared. Positivity appeared as brown coloration[21].

Positive cells for AFP show brown cytoplasmic staining. Positive cells for PCNA show brown nuclear staining. WT-1 expression appears as brown nuclear staining in podocytes. Negative control was done by the omission of primary antibodies. Positive control for each antibody was according to the manufacturer.

c. Electron microscopy

Specimens were immediately fixed in 2.5% glutaraldehyde for 2 hours at 4ºC (buffered with 0.1 M phosphate buffer, pH 7.4), washed in phosphate buffer, and then post-fixed in 1% osmium tetroxide for another one hour at 4ºC. The specimens were processed and embedded in resin. Semithin sections (1 µm) were stained with toluidine blue. Ultra-thin sections (70-90 nm) stained with uranyl acetate and lead citrate were examined with the transmission electron microscope[22]. This technique was done in the Electron Microscopy Unit at Assuit University.

Morphometric Studies

Using light microscopy Leica ICC50 Wetzlar (Germany), ten non-overlapped high-power fields(x400) were taken for each section at the Histology Department, Faculty of Medicine, Sohag University. Each field was analyzed using Image J1.51n software (National institutes of health USA Java 1.8.0_66 (32-bit):

1. The area percentage of collagen fibers with Masson trichrome was measured[23].
2. PAS-positive area percentage (delineating basement membranes and brush border) was measured[24].
3. The PCNA labeling index: (the number of positive cells / total cells counted in the field) x100[25].
4. The area percentage of AFP expression was measured
5. The number of WT-1 positive cells per glomerulus was counted[26]

Statistical Analysis

The statistical package SPSS, version 16.0 (SPSS Inc., Chicago, IL, USA) was used. Data were presented as means± standard deviation (SD) and the values were considered significant as *p-value* $\leq$ 0.05. One-way ANOVA test was used followed by Turkey's post-hoc test to compare the results between groups[27].

RESULTS

Body weight and relative kidney weight

There were non-significant differences in all control subgroups. The mean body weight and relative kidney

weight significantly decreased in DOX-treated groups (group IIa and group IIb) compared to the control. Further, group IIb significantly decreased versus group IIa. Both CeO2NPs and quercetin significantly increased in mean body weight and relative kidney weight compared to DOX-treated groups of the same duration but no significant difference was found between groups IIIa and IIIb versus groups IVa and IVb respectively. In group V, mean body weight and relative kidney weight significantly decreased compared to group IIb (Figures 2,3).

Biochemical studies

Serum urea, creatinine, and albumin

There were non-significant differences in all control subgroups. Significantly elevated serum urea and creatinine and decreased serum albumin were found in DOX-treated groups (groups IIa and IIb) compared to the control. Further, these changes were significantly different in group IIb versus group IIa (Table 1).

Both CeO2NPs and quercetin significantly decreased serum urea and creatinine, and increased serum albumin compared to DOX-treated groups of the corresponding time points. Groups IIIa and IIIb showed significantly decreased serum urea and creatinine versus groups IVa and IVb respectively. However, the difference in serum albumin level was non-significant between groups IIIa and IIIb versus groups IVa and IVb respectively. In group V, there was a significant increase in serum urea and creatinine while serum albumin concentration significantly decreased compared to group IIb (Table 1).

Lipid profile

There were non-significant differences in all control subgroups. Significantly elevated cholesterol and triglyceride levels while significantly decreased HDL were found in DOX-treated groups (groups IIa and IIb) compared to the control. Further, these changes were significantly different in group IIb versus group IIa (Table 2).

Both CeO2NPs and quercetin significantly decreased cholesterol and triglyceride levels and increased serum HDL compared to DOX-treated groups of the same duration. Groups IIIa and IIIb showed significantly decreased serum cholesterol and triglyceride levels and increased serum HDL versus groups IVa and IVb respectively. In group V, there were significantly elevated cholesterol and triglyceride levels while significantly decreased HDL compared to group IIb (Table 2).

Light microscopic results

H&E Stain

All the control subgroups showed the same histological results in the renal cortex. The renal corpuscle was formed of renal glomerulus surrounded by Bowman's capsule which is composed of parietal and visceral layers with the urinary space in between. The Proximal tubules showed a narrow lumen and their lining epithelium was formed of cuboidal cells with highly acidophilic cytoplasm and rounded vesicular nuclei. Apical brush borders were intact and regular. The distal tubules had a wide lumen. Low cuboidal cells with acidophilic cytoplasm and rounded vesicular nuclei were lining their lumen (Figure 4a).

DOX-treated groups (groups IIa and IIb) exhibited widened urinary space and congested glomerular capillaries. Tubular dilatation was observed both in the proximal and distal tubules. Some tubular cells had vacuolated cytoplasm and others appeared apoptotic with acidophilic cytoplasm and pyknotic nuclei. Degeneration of the apical brush border was observed in proximal tubules (Figure 4b). These changes were more prominent in group IIb than in IIa and seen in most tubules. Inflammatory cell infiltrations were seen. Intraluminal acidophilic casts in some tubules and some degenerated flattened epithelial cells were also seen in group IIb. Degeneration of the apical brush border was observed in most proximal tubules (Figure 4C).

DOX + CeO2NPs treated groups (groups IIIa and IIIb) showed an apparent decrease in the urinary space with less congested glomerular capillaries compared to DOX-treated groups of corresponding time points. Most proximal and distal tubules restored their normal shape in group IIIa (Figure 4d). Some tubular cells appeared vacuolated in group IIIb. The apical brush border was partially restored in most proximal tubules (Figure 4e).

In the DOX + quercetin groups (groups IVa, and IVb), reduced urinary space and less congested glomerular capillaries were observed as compared to DOX-treated groups of the corresponding time points. A few tubules in group Iva and some tubules in group IVb had lining cells with vacuolated cytoplasm. Degeneration of the apical brush border was observed in some proximal tubules (Figures 4f, g).

In group V, the degenerative changes mentioned in group II were markedly observed. Tubular casts and desquamated epithelium are seen in some tubules (Figure 4h).

Periodic acid Schiff technique (PAS)

All control subgroups showed the same results in the form of positive PAS reaction in the basement membranes of renal corpuscles and renal tubules and glomeruli. They showed regular brush borders of the proximal tubules (Figure 5a). There were non-significant differences in all control subgroups. Groups IIa and IIb showed significantly increased PAS area percentage compared to the control; being displayed as an increase in the intensity of PAS reaction with increased thickness of basement membranes of renal corpuscles, glomerular capillaries, and renal tubules. Irregular and destructed brush border was seen. Further, these changes were significant in group IIb versus group IIa (Figures 5b,c, i).

Both CeO2NPs and quercetin showed a significant decrease in PAS area percentage compared to DOX-

treated groups of corresponding time points. Further, group IIIa showed a significant decrease compared to group IVa. However, group IVb was non-significantly different versus group IIIb. Groups IIIa and IIIb showed a prominent decrease in the intensity of PAS reaction and thickness of basement membranes of renal corpuscles, glomerular capillaries, and renal tubules. Most proximal tubules showed regular brush borders in groups IIIa and IVa. Few proximal tubules showed irregular brush borders in group IIIb and group IVb (Figures 5 d,e, f, g, i). Group V exhibited a significantly increased PAS area percentage versus group IIb. The brush borders of the proximal tubules appeared irregular and interrupted (Figures 5h, i).

Masson trichrome stain

Examination of kidney sections of all control subgroups showed few collagen fibers around the renal corpuscle, between glomeruli and peritubular (Figure 6a). There were non-significant differences in all control subgroups. Groups IIa and IIb showed increased collagen fibers surrounding the renal corpuscle, between glomeruli and peritubular. Interstitial collagen fibers in between tubules more were prominent in group IIb. Significantly increased collagen fibers area percentage was found in DOX-treated groups (groups IIa and IIb) compared to the control. Further, these changes were significant in group IIb versus group IIa (Figures 6b, c, i).

Both CeO2NPs and quercetin showed a significant decrease in collagen fibers area percentage compared to DOX-treated groups of corresponding time points. Further, group IIIa and group IIIb showed a significant decrease compared to group IVa and group IVb respectively (Figures 6d, e, f, g, i); being demonstrated around the renal corpuscle, between glomeruli, peritubular and interstitial. Group V exhibited significantly increased collagen fibers surrounding the renal corpuscle, between glomeruli, peritubular and interstitial versus group IIb (Figure 6h, i).

Immunohistochemical results

a. PCNA antibody

All control subgroups showed similar results; few positive nuclei were seen in the glomeruli and renal tubule (Figure 7a). There were non-significant differences in all control subgroups. Significantly increased PCNA expression in DOX-treated groups (groups IIa and IIb) compared to the control; being demonstrated both in glomeruli and tubules. Further, these changes were significant in group IIb versus group IIa (Figures 7b, c, i). Both CeO2NPs and quercetin showed a significant decrease in PCNA expression compared to DOX-treated groups of corresponding time points. Further, group IIIa and group IIIb showed a significant decrease in PCNA positive nuclei compared to group IVa and group IVb respectively (Figures 7d, e, f, g, i). Group V showed significantly increased positive nuclei versus group IIb (Figure 7h, i).

b. AFP antibody

All control subgroups showed similar results in the form of more or less negative AFP expression in the glomeruli and tubules (Figure 8a). There were non-significant differences in all control subgroups. Significantly increased AFP expression area percentage in DOX-treated groups (groups IIa and IIb) as compared to the control; being demonstrated both in glomeruli and tubules. Further, these changes were significant in group IIb versus group IIa (Figures 8b,c, i). Both CeO2NPs and quercetin showed a significant decrease in AFP expression compared to DOX-treated groups of corresponding time points. Further, group IIIa and group IIIb showed a significant decrease in AFP expression compared to group IVa and group IVb respectively (Figures 8d, e, f, g, i). Group V showed significantly increased AFP expression versus group IIb (Figures 8h, i).

c. WT-1 antibody

All control subgroups showed similar results in the form of many WT-1 positive nuclei in the glomeruli representing podocytes (Figure 9a). Group IIa and group IIb showed significantly decreased WT-1 positive podocytes compared to the control. Further, these changes were significantly more in group IIb versus group IIa. (Figures 9b,c, i). Both CeO2NPs and quercetin showed significantly increased WT-1 count versus DOX-treated groups of the same duration. Further, Group IIIa and group IIIb showed a significant increase in WT-1 expression compared to, group IVa and group IVb respectively (Figure 9d,e,f, g, i). Group V showed significantly decreased WT-1 positive podocytes versus group IIb (Figures 9h, i).

Ultrastructural results

Ultrathin sections in the kidneys of all control subgroups showed that the glomerular capillaries were lined with fenestrated endothelial cells with the basal lamina. Podocytes were present surrounding the glomerular capillaries and had long processes and small secondary foot processes. The secondary processes were closely related to endothelial cells of the glomerular capillaries forming the filtration barrier. The glomerular basement membrane (GBM) appeared with a regular thickness (Figures 10 a,b). Cells of proximal tubules were cuboidal in shape with euchromatic nuclei and numerous microvilli. Basal parts had longitudinally arranged mitochondria with basal infoldings (Figure 10 c). Moreover, cells of distal tubules were cuboidal in shape with euchromatic nuclei with few short apical microvilli. The cytoplasm had numerous mitochondria that were longitudinally arranged with basal infoldings (Figure 10 d).

Group IIa showed a slightly irregular GBM. Podocyte showed effacement of foot processes which appeared as retraction, widening, and shortening of their foot processes with heterochromatic nucleus (Figures 11 a,b). Cells of the proximal tubule had partial loss microvilli with irregular basal infoldings with Mitochondria of different sizes

and shapes, heterochromatic nucleus, and cytoplasmic vacuoles (Figure 11 c). Also, cells of distal tubules showed irregular basal infoldings with many different shapes of mitochondria, cytoplasmic vacuoles, and heterochromatic nucleus (Figure 11d). These changes were more prominent in group IIb (Figure 12). In group IIb, GBM was seen of irregular thickness and podocyte showed more prominent effacement of foot processes with indented heterochromatic nucleus (Figures 12a,b). In addition to the changes mentioned in group IIa, megamitochondria and indented heterochromatic nuclei were seen in proximal and distal tubules of group IIb (Figures 12 c,d).

Group IIIa showed slightly irregular GBM thickness and attenuated effacement of foot processes of podocyte. Podocyte had euchromatic nucleus (Figures 13 a, b). Cells of proximal tubule had partial loss of microvilli with well-defined basal infoldings, mitochondria arranged in between basal infoldings, and euchromatic nucleus (Figure 13c). Moreover, Cells of distal tubule cells were more or less similar to control with numerous elongated mitochondria that are longitudinally arranged within the basal infoldings, euchromatic nucleus (Figure 13d). Group IIIb showed slight irregular GBM thickness and attenuated effacement of foot processes of podocyte. Podocyte had euchromatic nucleus (Figures 14 a,b). Cells of proximal tubule had partial loss of microvilli with mitochondria of different sizes and shapes in-between basal infoldings and euchromatic nucleus and some vacuoles (Figure 14c). Cells of distal tubule were more or less similar to control except one cell had indented nucleus (Figure 14d).

Group IVa showed slightly irregular GBM thickness and decreased effacement of podocyte foot processes (Figures 15 a,b). Cells of the proximal tubule had regular microvilli partially lost in small areas, mitochondria arranged in between well-defined basal infoldings and some vacuoles. Cells had euchromatic nuclei (Figure 15c). Cells of distal tubules were more or less similar to control (Figure 15d). Similar findings were seen in group IVb with more effacement (Figures 16a,b), some vacuoles in proximal tubular cells (Figure 16c) and irregularly arranged mitochondria of different shapes in the basal part of the distal tubular cell (Figure 16d).

Group V showed marked irregular thickening of GBM and extensive effacement of podocyte foot processes. Podocyte had euchromatic nucleus. (Figures 17 a,b). Cells of proximal tubule had disrupted microvilli and ill-defined basal infoldings with heterochromatic nuclei, irregular nuclear membrane, and clumps of peripheral heterochromatin (Figure 17c). Cells of distal tubules showed ill-defined basal infoldings with numerous mitochondria of different shapes and heterochromatic small nucleus (Figure 17d).

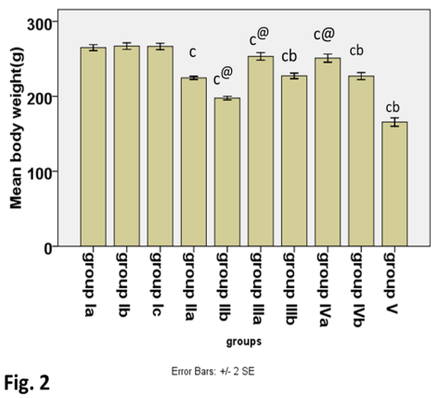

Fig. 2

Fig. 2: Histogram showing the mean animal body weight in different groups. C: significant compared to group Ia, @ Significant compared to group IIa, b: significant compared to group IIb, one-way ANOVA followed by Turkey's post-hoc test

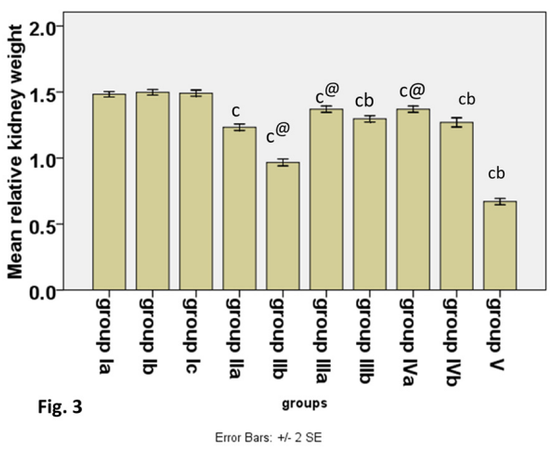

Fig. 3

Fig. 3: Histogram showing the mean relative kidney weight in different groups. C: significant compared to group Ia, @ Significant compared to group IIa, b: significant compared to group IIb, one-way ANOVA followed by Turkey's post-hoc test

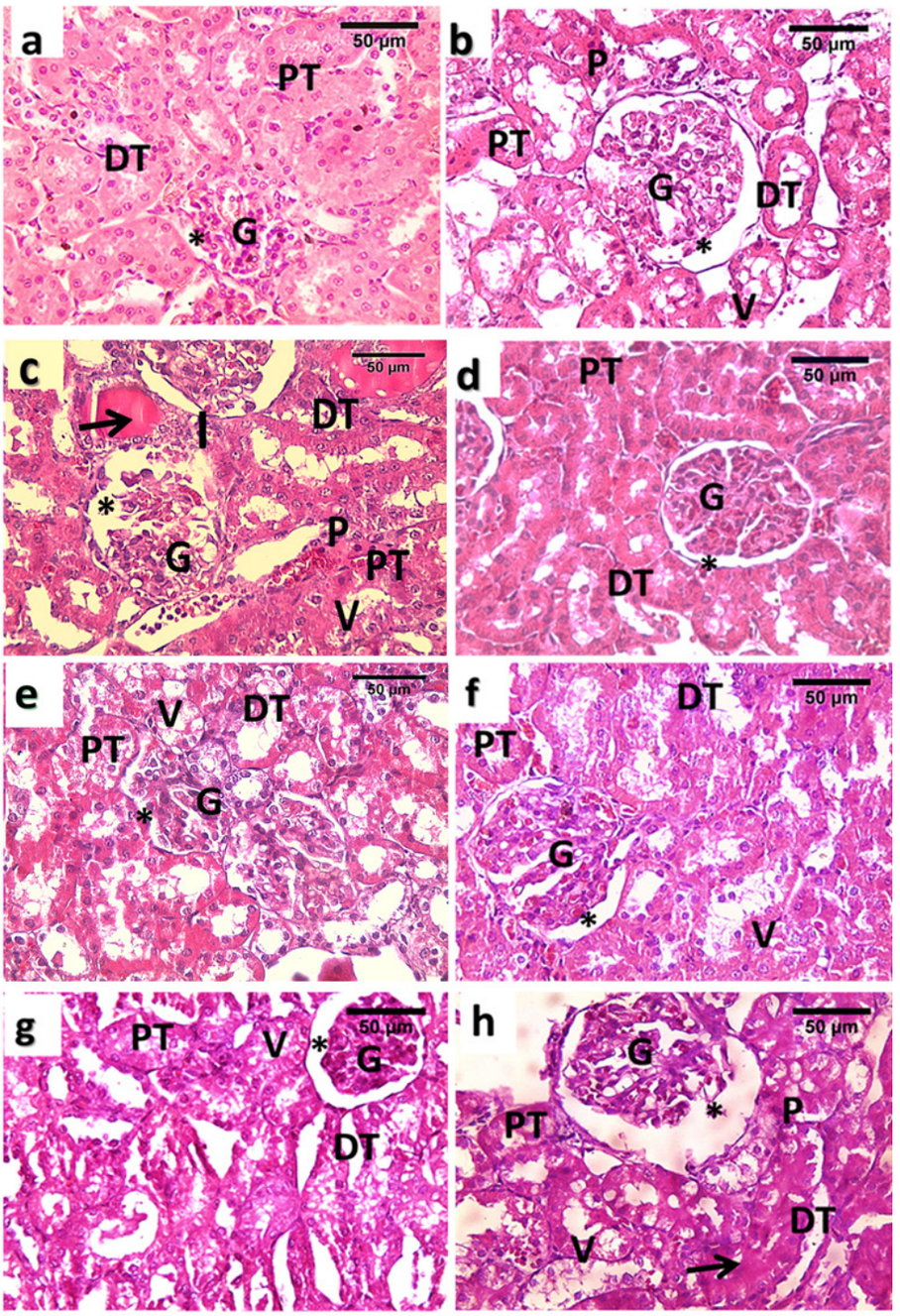

Fig. 4

Fig. 4: Photomicrographs of kidney sections stained with H&E (a) Group I showing; renal corpuscle with normal glomerular capillaries (G) and urinary space (star), proximal tubule (PT) has a narrow lumen and lined with cuboidal cells with vesicular nuclei and intact brush border. The distal tubule (DT) has a wide lumen and is lined with cuboidal cells with vesicular nuclei and acidophilic cytoplasm. (b) Group IIa and (c) group IIb show congestion of glomerular capillaries (G), and widening of urinary space (star). The lining epithelium of the proximal tubule (PT) and distal tubule (DT) showing degenerated flattened epithelial cells, vacuolated cytoplasm (V), and apoptotic cells (P). (c) These degenerative changes are more prominent with interstitial inflammatory cell infiltration (I) and intratubular casts (arrow). Note the dilated lumen of tubules and loss of brush border in PT. (d) Group IIIa is more or less normal. (e) Group IIIb decreased urinary space (star) and degenerative changes with some vacuolated cells (V (f) Group IVa, and (g) group IVb showing decreased urinary space (star), with some vacuolated cells(V) (h) group V showing markedly dilated urinary space (star), degenerative changes are extensive. Tubular casts (arrow) and desquamated epithelium are seen in some tubules. Glomerular capillaries (G), proximal tubule (PT). Distal tubule (DT). Note the dilated lumen of tubules and loss of brush border in PT. apoptotic cells (P) (H&E x 200, scale bar=50).

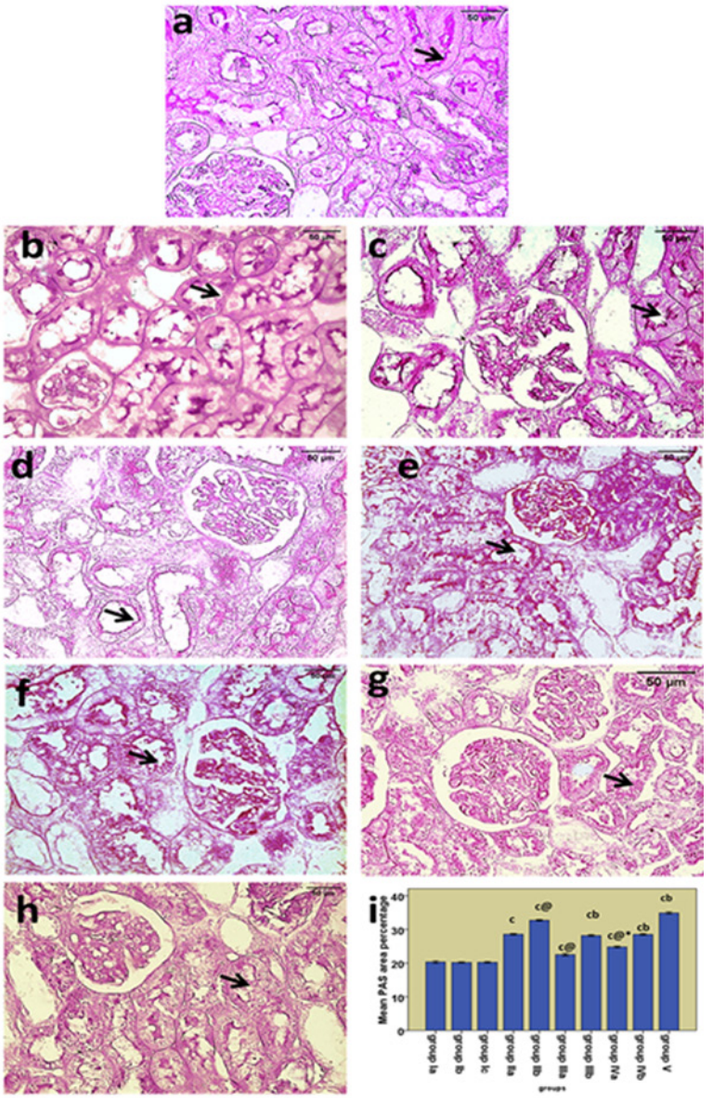

Fig. 5

Fig. 5: Photomicrographs of kidney sections stained with PAS (a) Control showing; a positive reaction in basement membranes of renal corpuscles, and renal tubules. Regular brush border of PT (arrow). (b) Group IIa and (c) group IIb showing; increased intensity of the reaction in basement membranes of the renal corpuscles, Note interrupted degenerated brush border of P.T (arrow). (d) Group IIIa, (e) group IIIb, (f) group IVa and (g) group IVb showing decrease intensity of positive reaction in basement membranes of renal corpuscles, note regular brush border of P.T (arrow) in most tubules except in few tubules in (e,g). (h) Group V shows increased intensity of the reaction in basement membranes of the renal corpuscles and renal tubules. Note degenerated brush border of PT (arrow). (PAS x400, scale bar=50). (i) Histogram showing PAS area percentages in different groups. C: significant compared to group Ia, @ Significant compared to group IIa, b: significant compared to group IIb, *: significant compared to group IIIa, #: significant compared to group IIIb. One-way ANOVA followed by Turkey's post-hoc test

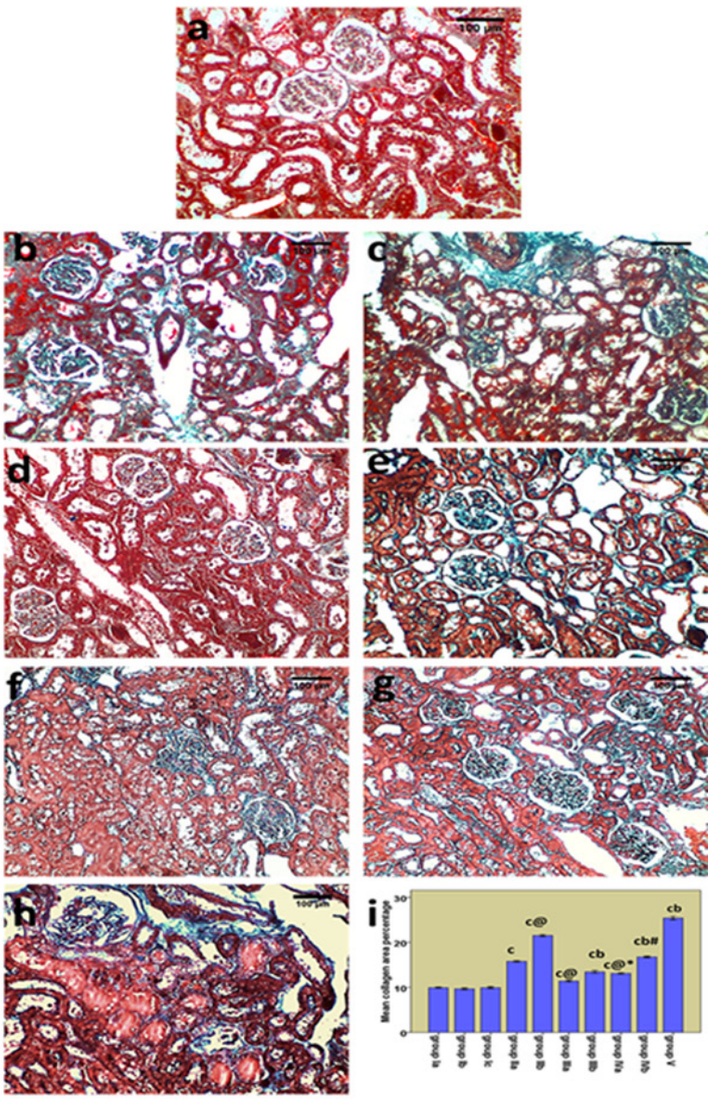

Fig. 6

Fig. 6: Photomicrographs of kidney sections stained with Masson trichrome (a) control group showing few collagen fibers around the glomeruli, and renal tubules (b) group IIa and (c) group IIb showing an increase in collagen fibers around the glomeruli and tubules and in renal interstitium which is more prominent in group IIb. (d) Group IIIa,(e) group IIIb, (f) group IVa and (g) group IVb showing decreased collagen fibers around the glomeruli, and tubules, and in renal interstitium h) Group V showing markedly increased collagen fibers around the glomeruli, and tubules and in the renal interstitium (Masson trichrome x200, scale bar=100). (i) Histogram showing collagen fibers area percentages in different groups. C: significant compared to group Ia, @ Significant compared to group IIa, b: significant compared to group IIb, *: significant compared to group IIIa, #: significant compared to group IIIb. One-way ANOVA followed by Turkey's post-hoc test

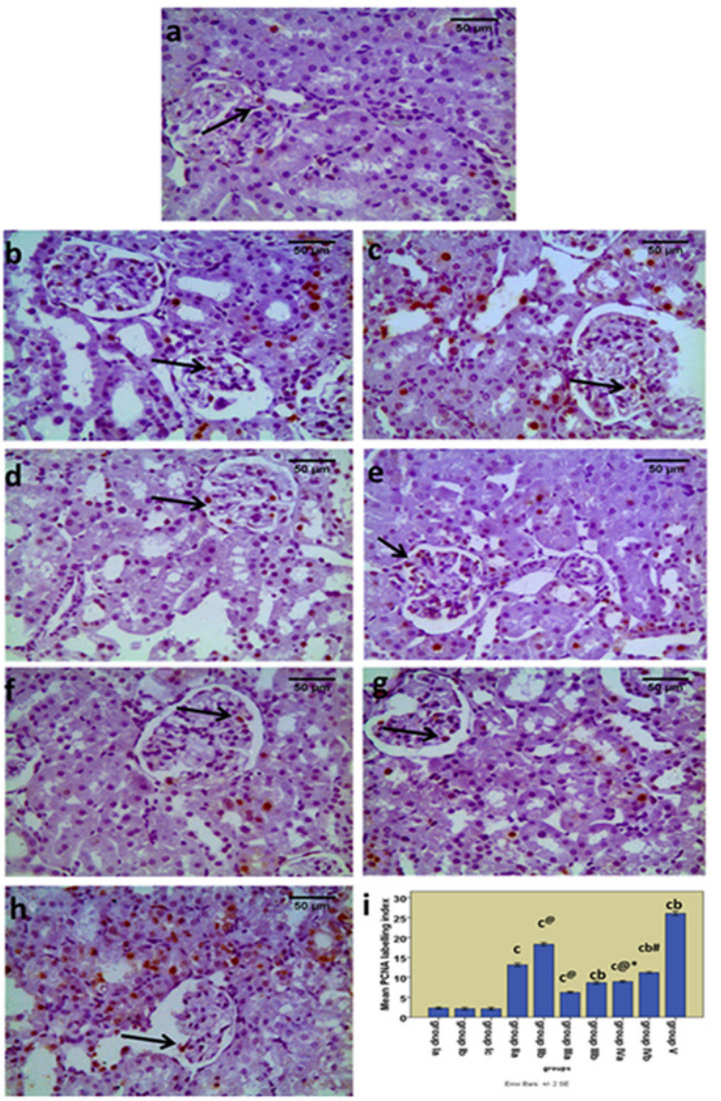

Fig. 7

Fig. 7: Photomicrographs of kidney sections immunostained with PCNA antibody. a) Control showing few PCNA positive nuclei in the glomeruli (arrow) and renal tubule. b) Group IIa showing increased PCNA positive nuclei and c) group IIb showing many PCNA positive nuclei in the glomeruli(arrow) and tubules. d) Group IIIa and e) group IIIb showing few PCNA positive nuclei in the glomeruli (arrow) and tubules. f) Group IVa and g) group IVb showing some PCNA positive nuclei in the glomeruli (arrow) and tubules h) Group V showing markedly increased positive nuclei in the glomeruli (arrow) and tubules (PCNA antibody×400, scale bar=50). (i) Histogram showing PCNA labeling index in different groups. C: significant compared to group Ia, @ Significant compared to group IIa, b: significant compared to group IIb, *: significant compared to group IIIa, #: significant compared to group IIIb. One-way ANOVA followed by Turkey's post-hoc test.

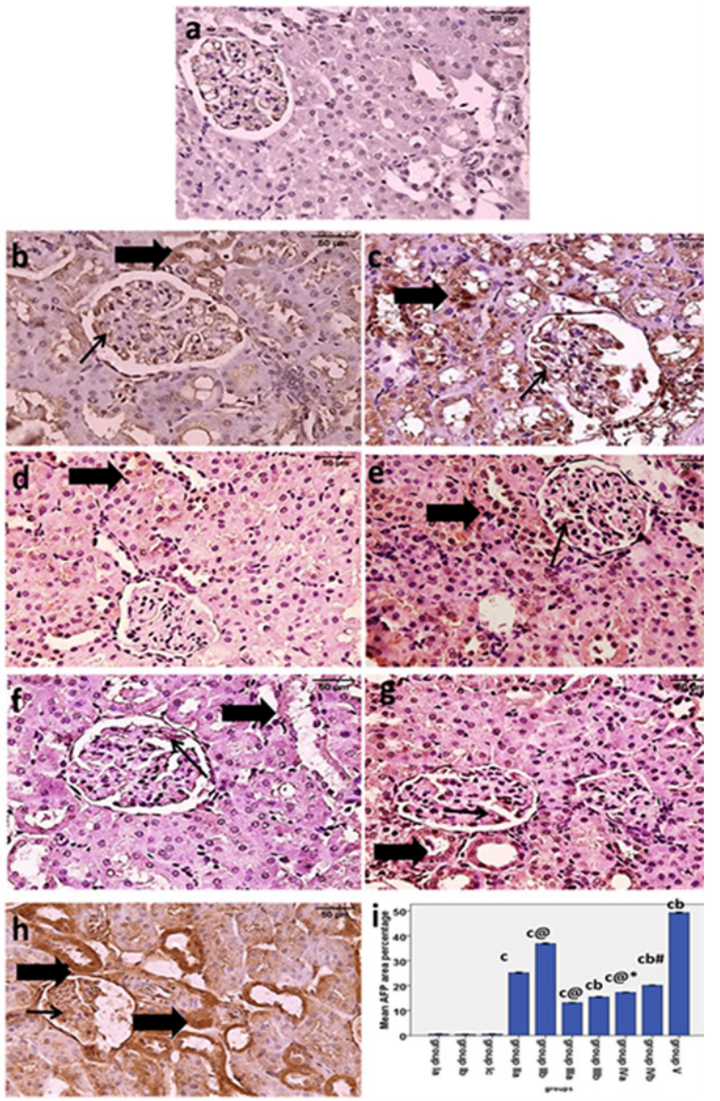

Fig. 8

Fig. 8: Photomicrographs of kidney sections immunostained with AFP antibody. a) Control showing negative AFP in the glomeruli and tubules. b) Group IIa and c) group IIb showing an increase in AFP positive cells in the glomeruli (thin arrow) and tubules (thick arrow) which is more prominent in group IIb. (d) Group IIIa,(e) group IIIb, (f) group IVa and (g) group IVb showing decreased AFP positive cells (h) Group V showing increased AFP positive cells compared to group IIb. Positive cells in the glomeruli (thin arrow) and tubules (thick arrow) (AFP antibody×400, scale bar=50). (i) Histogram showing area percentages of AFP expression in different groups. C: significant compared to group Ia, @ Significant compared to group IIa, b: significant compared to group IIb, *: significant compared to group IIIa, #: significant compared to group IIIb. One-way ANOVA followed by Turkey's post-hoc test.

Fig. 9

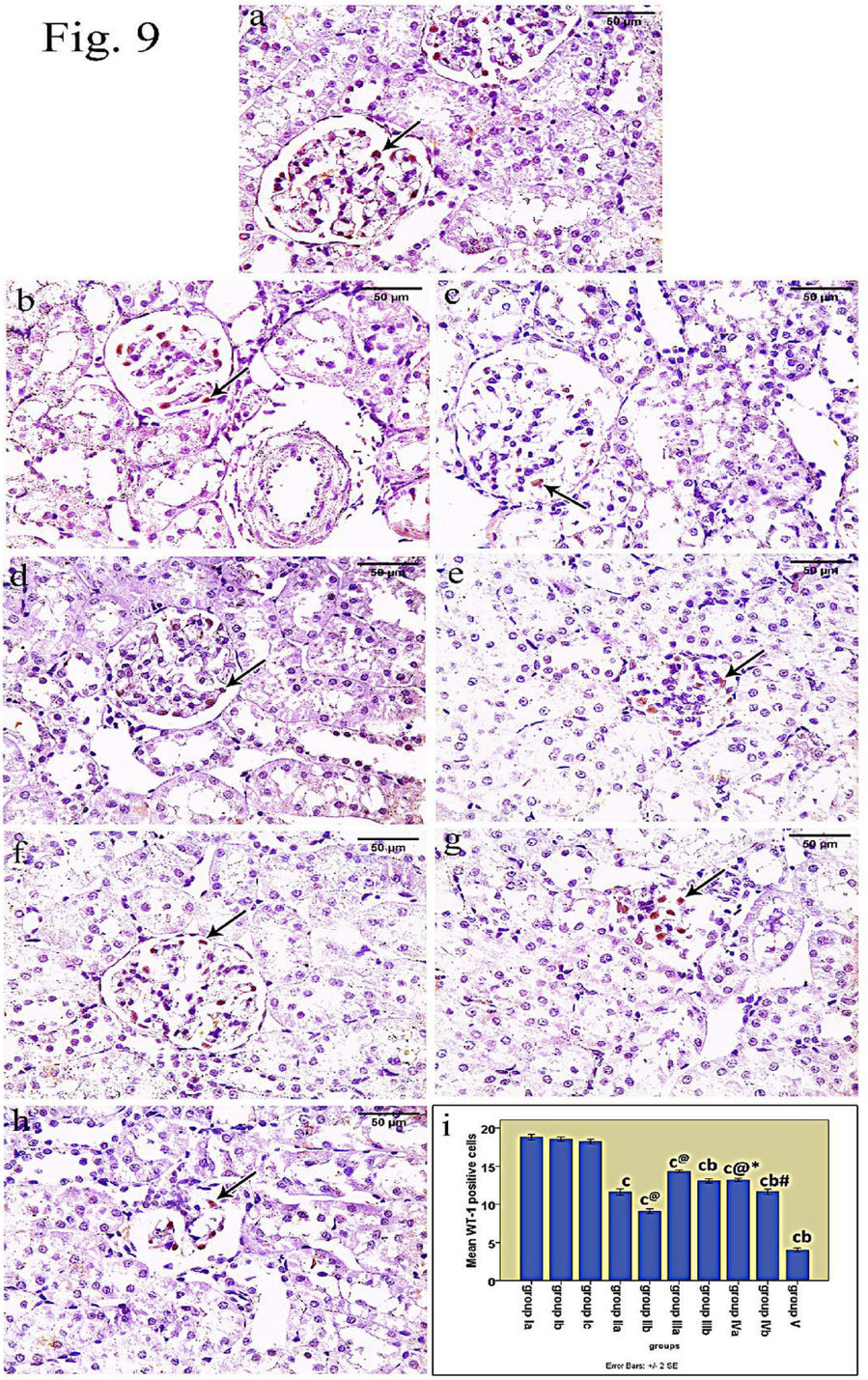

Fig. 9: Photomicrographs of kidney sections immunostained with WT-1 antibody of a) control group showing many WT-1 positive nuclei in the glomeruli b) group IIa and c) group IIb showing few WT-1 positive nuclei in the glomeruli d) group IIIa and e) group IIIb showing increased WT-1 positive nuclei in the glomeruli.f) group IVa and g) group IVb showing some WT1 positive nuclei in the glomeruli h) groupV showing markedly decreased WT-1 positive nuclei.(positive nuclei, arrow) (WT-1 a ntibody×400, scale bar=50). (i) Histogram showing the mean number of WT-1 positive nuclei in different groups. C: significant compared to group Ia, @ Significant compared to group IIa, b: significant compared to group IIb, *: significant compared to group IIIa, #: significant compared to group IIIb. One-way ANOVA followed by Turkey's post-hoc test.

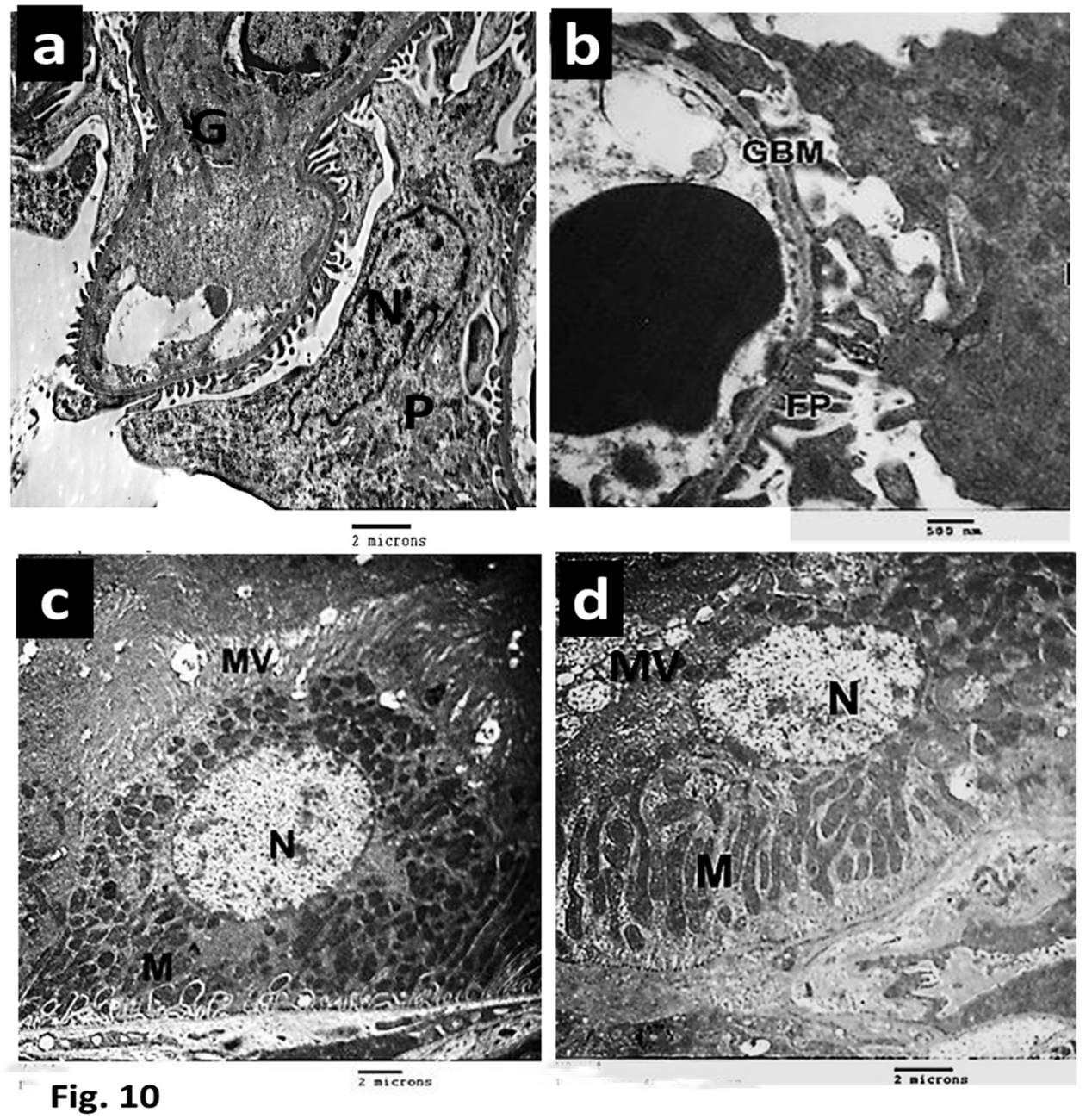

Fig. 10: Electron micrographs of ultrathin sections of the control group showing (a), (b) euchromatic Nucleus (N) of podocyte (P), glomerular capillary (G), regular glomerular basement membrane (GBM), and no effacement of the foot processes (FP). (c) Proximal tubular cell with regular numerous apical microvilli (MV), basal infoldings in which the mitochondria (M) are longitudinally arranged with rounded and euchromatic nucleus (N). (d) Distal tubular cell with basal infoldings in which the elongated mitochondria (M) are longitudinally arranged with rounded and euchromatic nucleus (N) and few short microvilli (MV). (TEM: a x4800, b x14000, c x3600 and d x6000, a,c,d: Scale bar =2 um, b scale bar =500 nm).

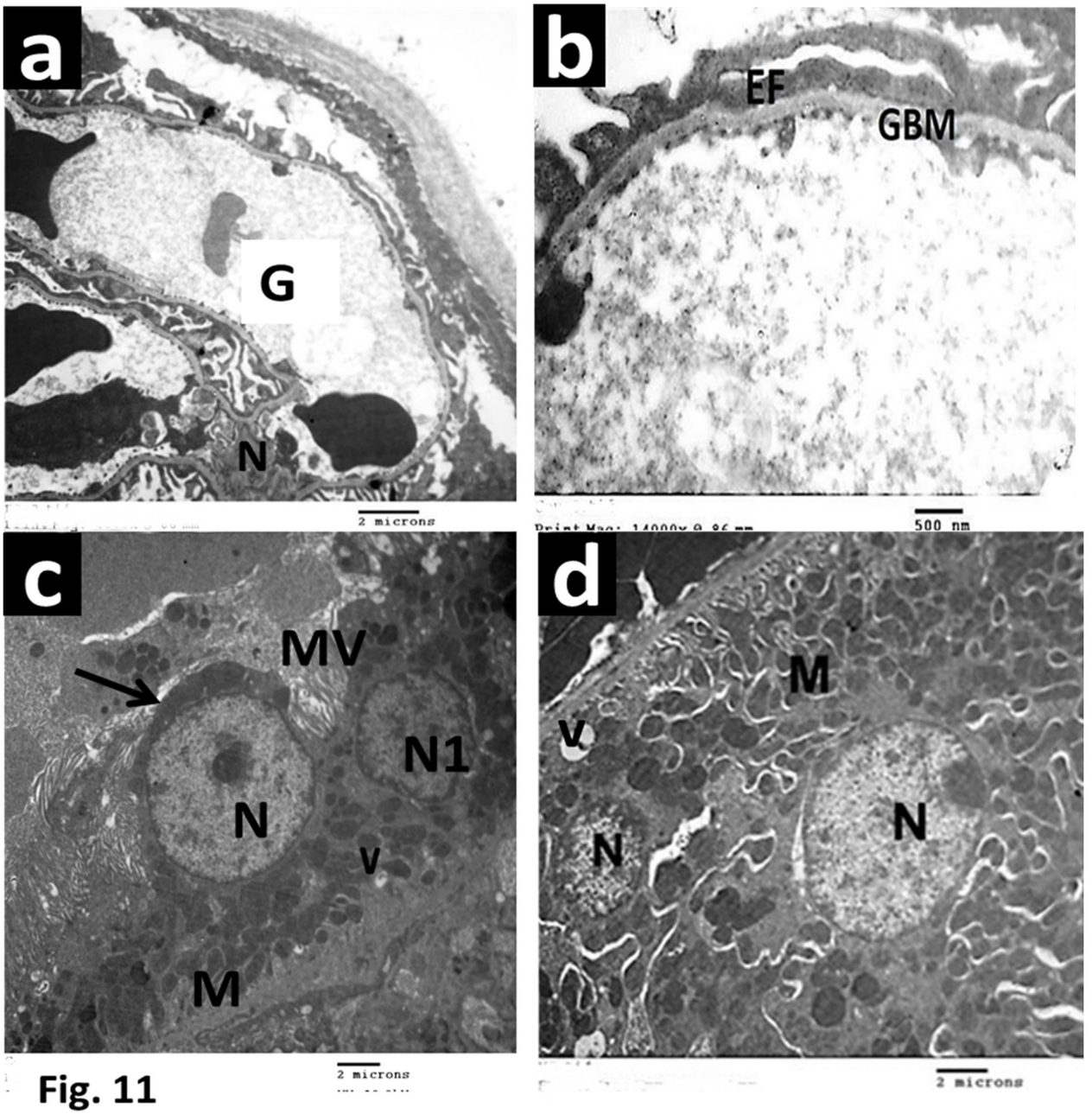

Fig. 11: Electron micrographs of ultrathin sections of group IIa showing;
(a), (b) heterochromatic indented nucleus (N) of podocyte, glomerular capillary (G), slight irregular glomerular basement membrane (GBM), and effacement of the foot processes (EF). (c) proximal tubular cell with partial loss (arrow) in apical microvilli (MV), basal infoldings in which numerous mitochondria of different shapes and sizes (M) are present, vacuole (V) and heterochromatic nucleus (N), and another shrunken cell with indented heterochromatic nucleus (N1). (d) Distal tubular cell with basal infoldings in which numerous different shaped mitochondria (M) are arranged and heterochromatic nucleus (N). vacuole (V)
(TEM: a x4800, b x 14000, c x 3600 and d x 6000, a,c,d: Scale bar =2 um, b scale bar =500 nm).

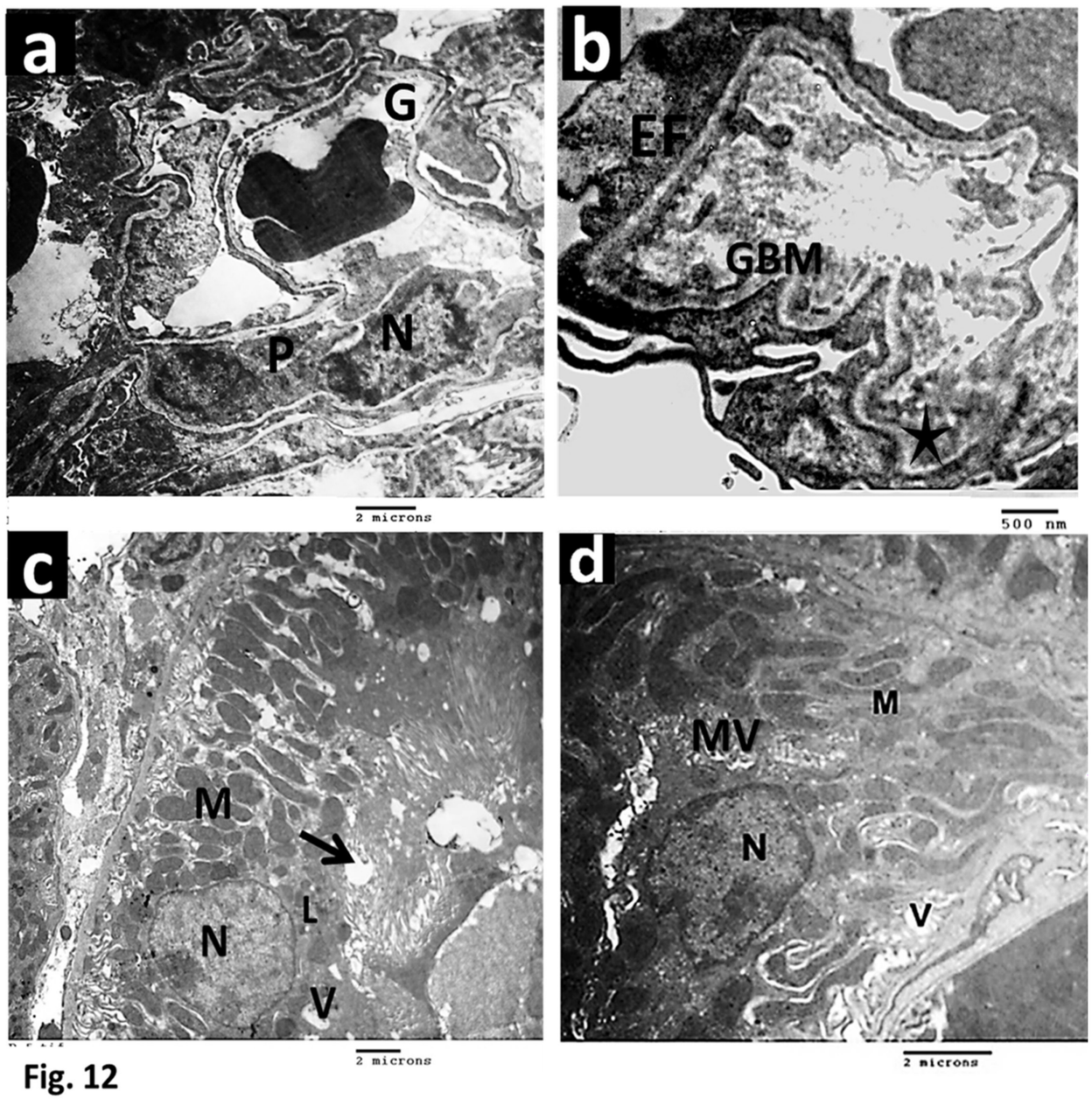

Fig. 12

Fig. 12: Electron micrographs of ultrathin sections of group IIb showing (a), (b) heterochromatic indented nucleus (N) of podocyte (P), glomerular capillary (G), irregularity (star) in the glomerular basement membrane (GBM), and effacement of the foot processes (EF). (c) Proximal tubular cell with distorted apical microvilli (arrow), with numerous mega mitochondria (M), vacuoles(V), and heterochromatic nucleus (N). Lysosomes (L)(d) Distal tubular cell with irregular basal infoldings in which numerous swollen mitochondria of different sizes and shapes (M), vacuoles(V), and heterochromatic nucleus (N) with the irregular nuclear envelope. Few short apical microvilli(MV)
(TEM: a x4800, b x 14000, c x3600 and d x6000, a,c,d: Scale bar =2 um, b scale bar =500 nm).

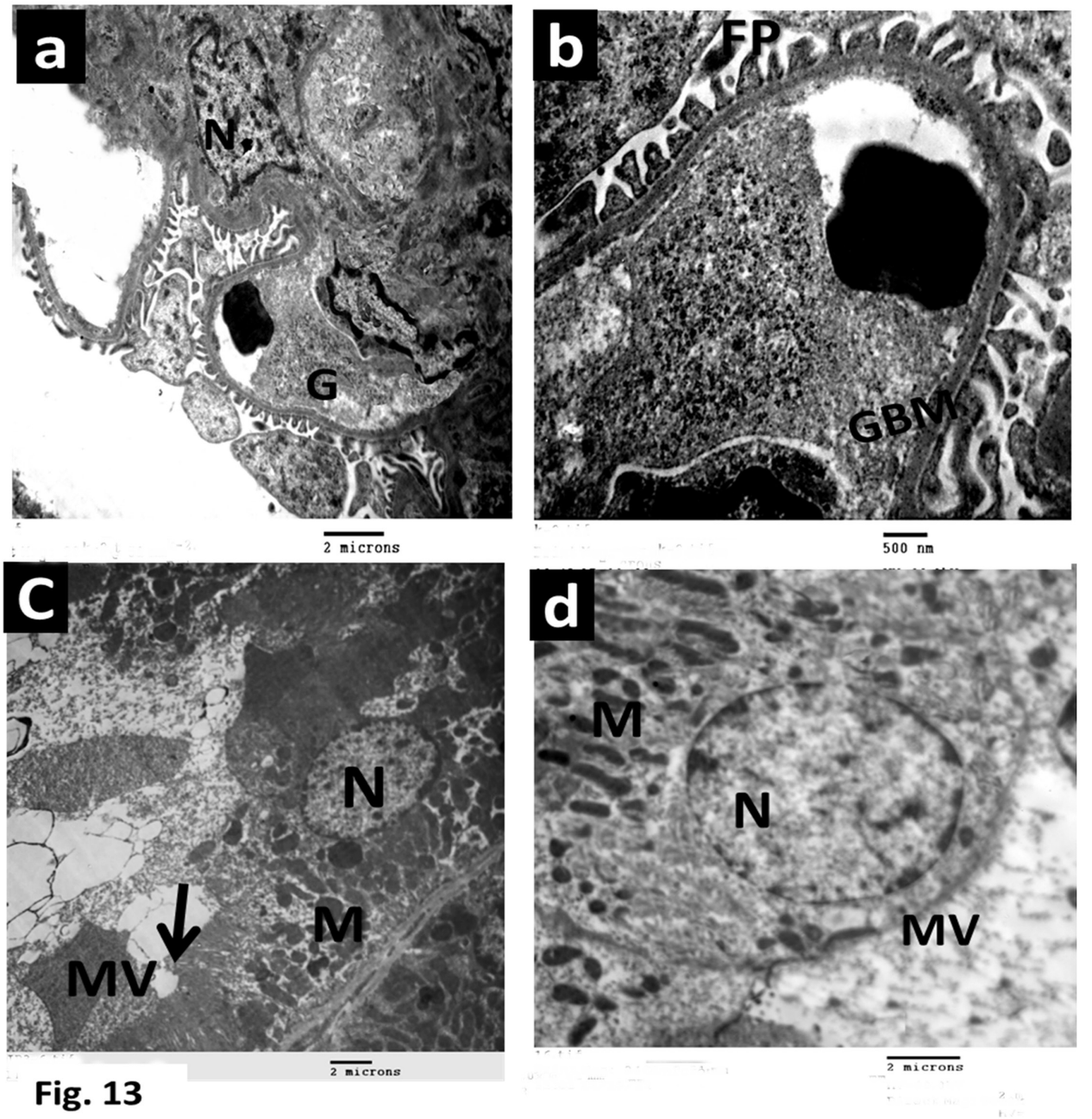

Fig. 13: Electron micrographs of ultrathin sections of group IIIa showing; (a), (b) euchromatic Nucleus (N) of podocyte, glomerular capillary (G), slight irregular glomerular basement membrane (GBM), and decreased effacement of the foot processes (FP). (c) Proximal tubular cell with partial loss (arrow) of apical microvilli (MV), basal infoldings with numerous longitudinal arranged mitochondria (M), euchromatic nucleus (N). (d) Distal tubular cells with numerous elongated mitochondria (M) longitudinal arranged within basal infoldings and euchromatic nucleus (N) and few apical short microvilli (MV). (TEM: a x4800, b x14000, c x3600 and d x6000, a,c,d: Scale bar =2 um, b scale bar= 500nm).

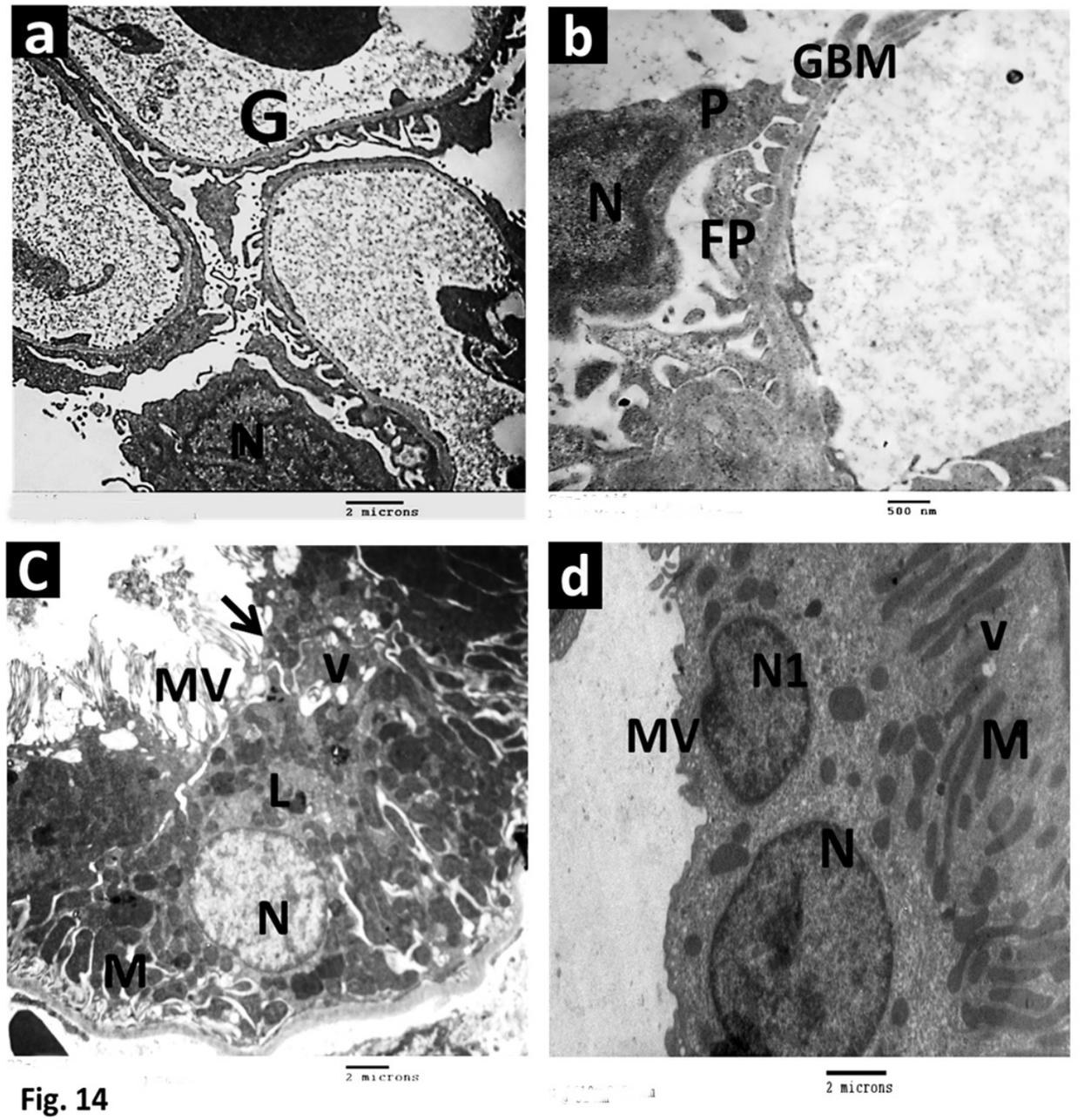

Fig. 14: Electron micrographs of ultrathin sections of group IIIb showing; (a), (b) euchromatic Nucleus (N) of podocyte (P), glomerular capillary (G), slight irregular glomerular basement membrane (GBM), and decreased effacement of the foot processes (FP). (c) Proximal tubular cell with partially distorted (arrow) apical microvilli (MV), well-defined basal infoldings in which the numerous mitochondria are arranged (M), and euchromatic nucleus (N). vacuole(V) (d) Distal tubular cells with numerous elongated mitochondria (M) within basal infoldings and euchromatic nucleus (N). Another cell with indented nucleus (N1). Few short apical microvilli (MV). vacuole(V)
(TEM: a x4800, b x14000, c x3600 and d x6000, a,c,d: Scale bar =2 um, b scale bar =500 nm).

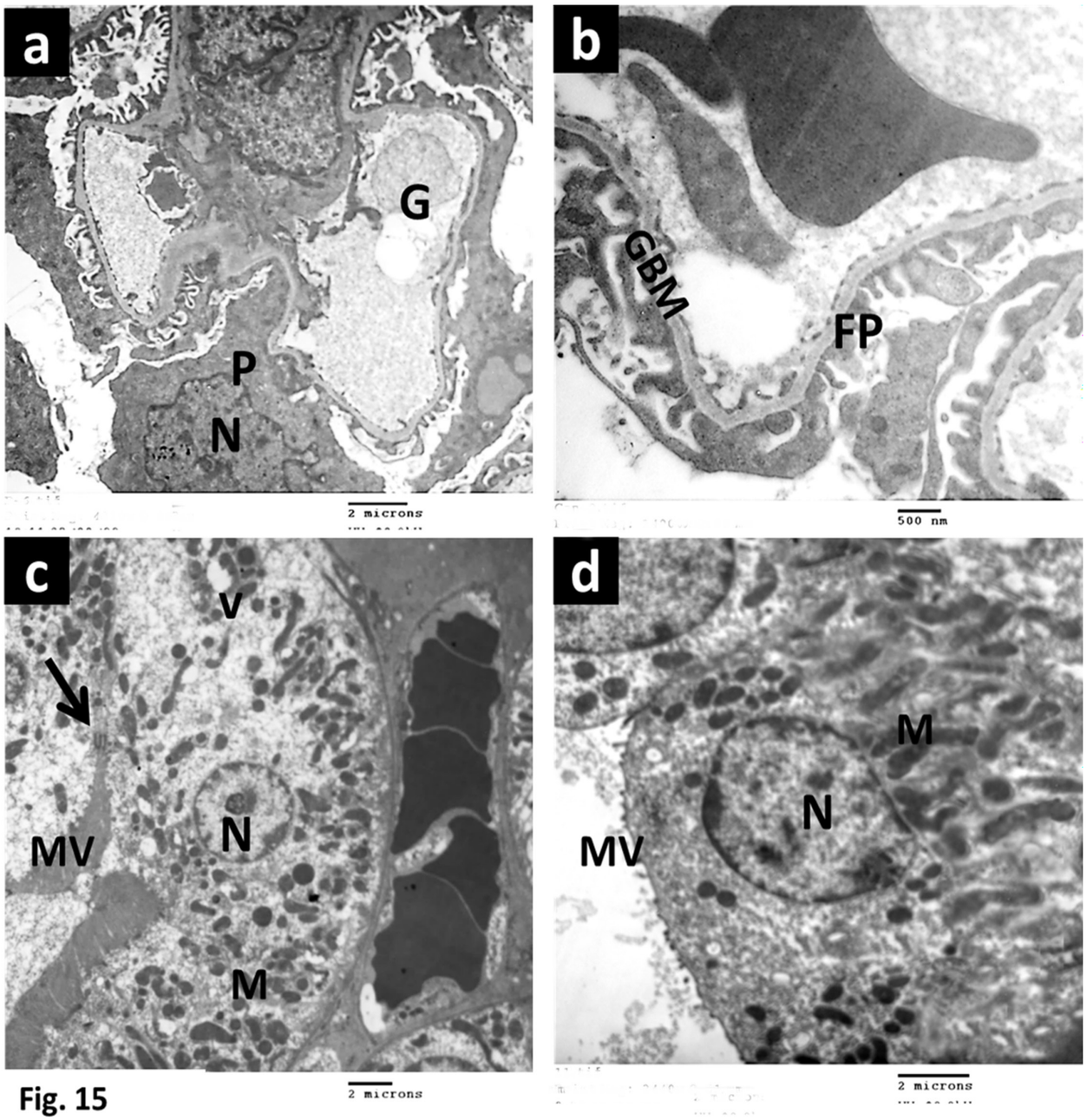

Fig. 15

Fig. 15: Electron micrographs of ultrathin sections of group IVa showing; (a), (b) euchromatic Nucleus (N) of podocyte (P), glomerular capillary (G), slight irregular glomerular basement membrane (GBM), and decreased effacement of the foot processes (FP). (c) Proximal tubular cell with apical microvilli (MV) but lost MV in small areas(arrow) well-defined basal infoldings in which numerous mitochondria (M). euchromatic nucleus (N). vacuole(V). (d) Distal tubular cells with numerous elongated mitochondria (M) longitudinally arranged within basal infoldings and euchromatic nucleus (N). Few short apical microvilli (M V)

(TEM: a x4800, b x14000, c x3600 and d x6000, a,c,d: Scale bar =2 um, b scale bar =500 nm).

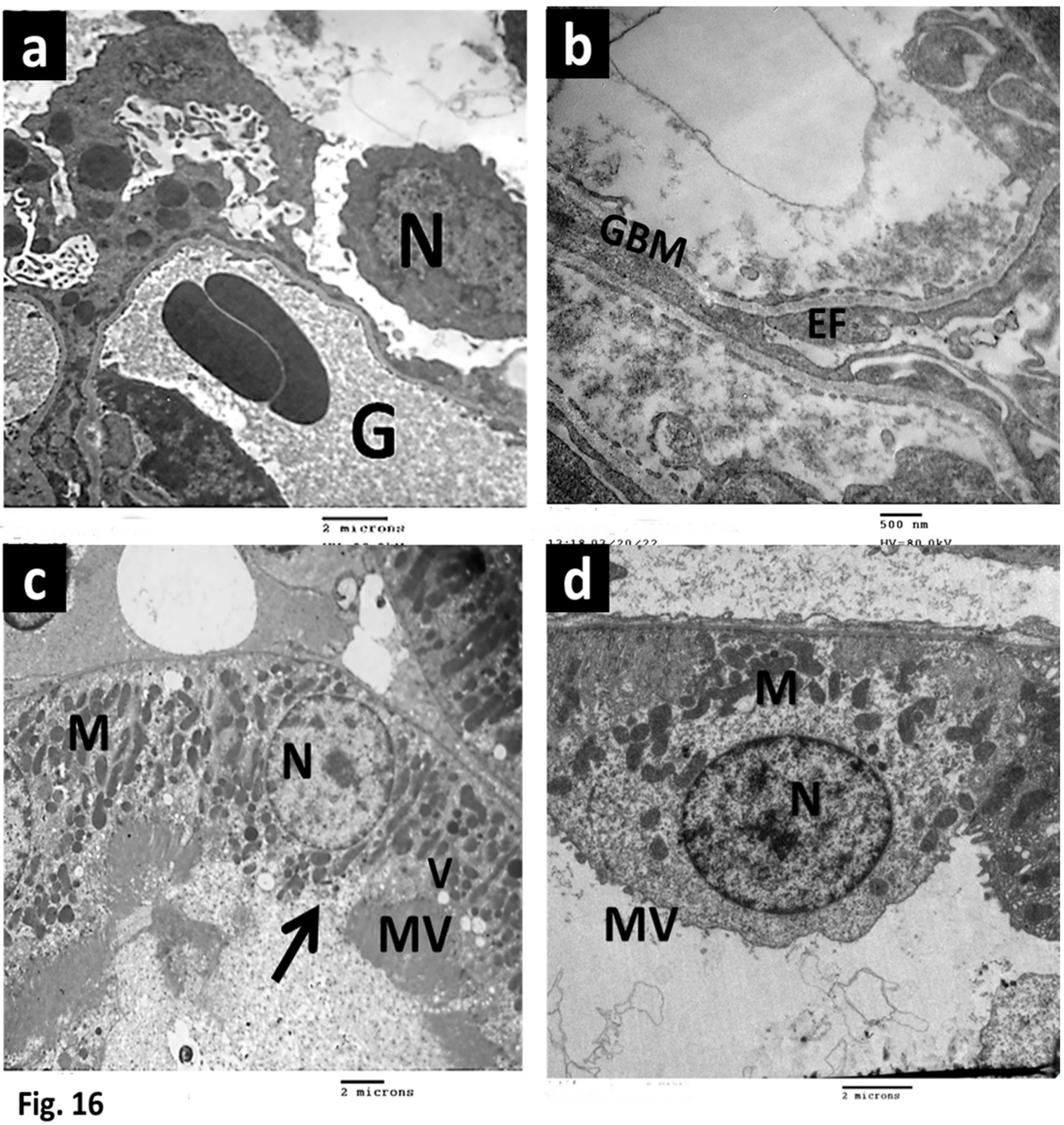

Fig. 16

Fig. 16: Electron micrographs of ultrathin sections of group IVb showing; (a), (b) euchromatic Nucleus (N) of podocyte, glomerular capillary (G), slightly irregular glomerular basement membrane (GBM), and effacement of the foot processes (EF). (c) Proximal tubular cell with partial regular apical microvilli (MV), partial loss of microvilli (arrow), well-defined basal infoldings in which numerous mitochondria are arranged (M) longitudinally and euchromatic nucleus(N). vacuoles (V) (d) Distal tubular cell with numerous mitochondria (M) within basal infoldings and euchromatic nucleus (N). few short apical microvilli (MV)

(TEM: ax4800, b x14000, c x3600 and d x6000, a,c,d: Scale bar =2 um, b scale bar =500 nm).

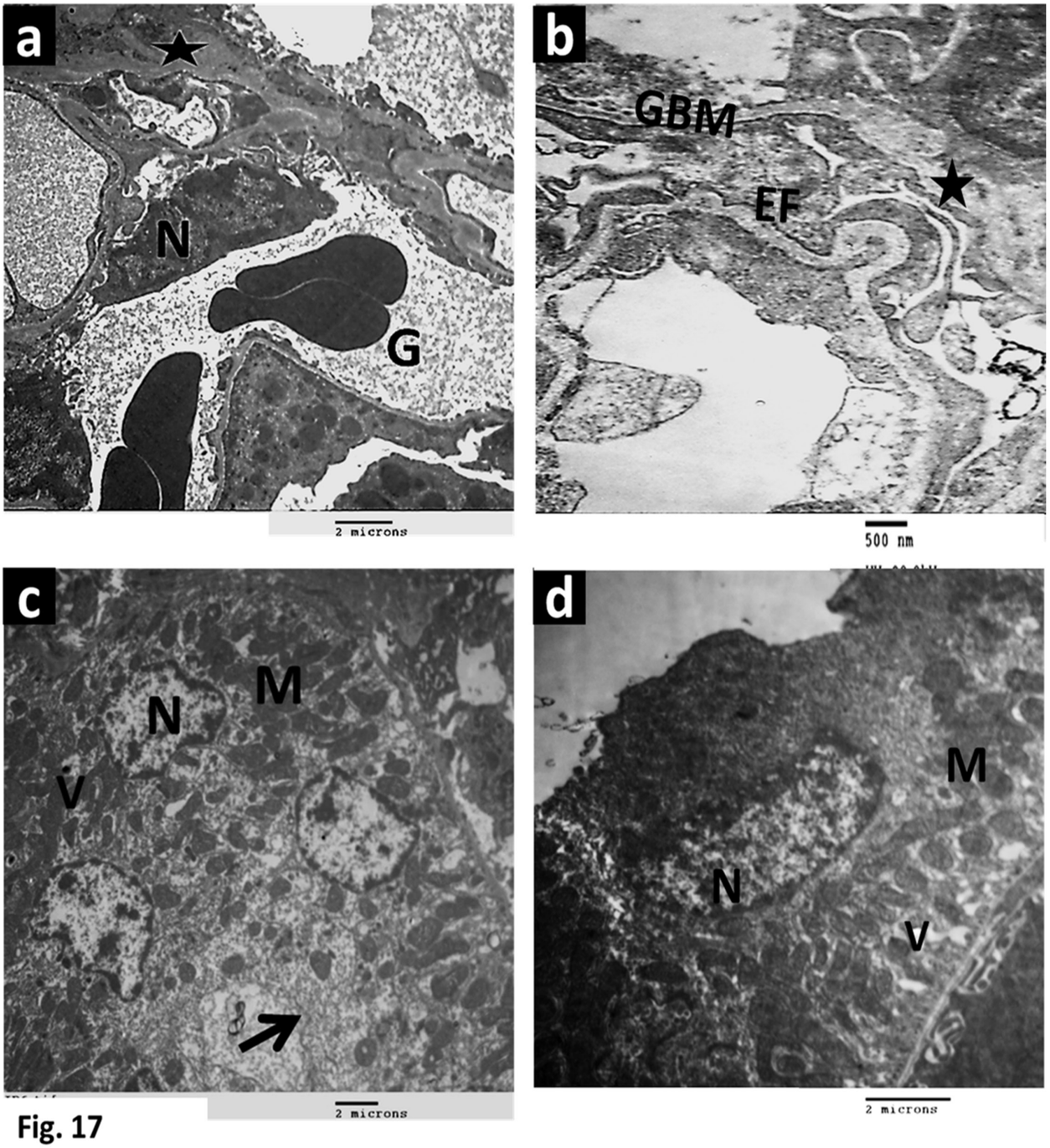

Fig. 17

Fig. 17: Electron micrographs of ultrathin sections of group V showing; (a), (b) marked irregular thickness (star) of the glomerular basement membrane (GBM), glomerular capillary (G), indented heterochromatic nucleus (N) of podocyte and marked effacement of the foot processes of podocyte (EF) (c) Proximal tubular cell with markedly disrupted apical microvilli (arrow), vacuoles (V), distorted mitochondria (M), ill-defined basal infoldings and heterochromatic nucleus (N) with peripheral clumps of heterochromatin and irregular nuclear envelope. (d) Distal tubular cell with numerous different shaped mitochondria (M) and heterochromatic nucleus with an indented nuclear envelope (N), vacuoles (V).
(TEM: a x4800, b x14000, c x3600 and d x6000, a,c,d: Scale bar =2 um, b scale bar =500 nm).

Table 1: Mean serum urea, creatinine and albumin in all studied groups

	Serum Urea(mg/dl) mean±SD	Serum Creatinine (mg/dl) mean±SD	Serum Albumin (mg/dl) mean±SD
Group Ia	15.87±8.52	0.59±.15	4.100±.64
Group Ib	16.07±8.43	0.59±.14	4.117±.66
Group Ic	18.00±8.75	0.53±.13	4.073±.73
Group IIa	49.03±3.23^{c}	1.39±.15^{c}	2.420±.32^{c}
Group IIb	66.90±4.10$^{c@}$	2.110±.38$^{c@}$	1.477±.39$^{c@}$
Group IIIa	25.90±2.81$^{c@}$	0.677±.12$^{@}$	3.741±.41$^{@}$
Group IIIb	39.27±3.37^{cb}	1.023±.13^{cb}	3.260±.32^{cb}
Group IVa	35.37±2.95$^{c@*}$	1.007±.08$^{c@*}$	2.267±.31c@
Group IVb	47.73±5.85$^{cb\#}$	1.887±.06$^{cb\#}$	3.037±.26^{cb}
Group V	89.80±4.40^{cb}	3.154±.23^{cb}	0.667±.82^{cb}

C: significant compared to group Ia, @ Significant compared to group IIa, b: significant compared to group IIb, *: significant compared to group IIIa, #: significant compared to group IIIb. One-way ANOVA followed by Turkey's post-hoc test

Table 2: Mean blood cholesterol, high-density lipoproteins and triglycerides in all studied groups

	Cholesterol (mg/dl) mean±SD	High-density lipoproteins (mg/dl) mean±SD	Triglycerides (mg/dl) mean±SD
Group Ia	22.20±9.03	73.77±16.54	38.16±18.40
Group Ib	21.70±9.28	71.70±13.88	38.17±18.00
Group Ic	21.30±9.39	72.53±14.85	38.15±18.50
Group IIa	50.10±3.28^{c}	48.90±9.24^{c}	155.73±9.78^{c}
Group IIb	60.23±3.21$^{c@}$	34.90±3.44$^{c@}$	185.80±9.20$^{c@}$
Group IIIa	24.40±3.52$^{@}$	70.07±10.19$^{@}$	38.47±10.579$^{@}$
Group IIIb	33.57±3.28^{cb}	61.43±4.27^{cb}	55.50±8.94^{cb}
Group IVa	30.47±1.85$^{c@*}$	62.83±4.72$^{c@*}$	61.67±14.23$^{c@*}$
Group IVb	39.80±3.10$^{cb\#}$	48.23±1.54$^{cb\#}$	87.10±6.25$^{cb\#}$
Group V	75.00±4.06^{cb}	14.43±3.02^{cb}	220.07±10.08^{cb}

C: significant compared to group Ia, @ Significant compared to group IIa, b: significant compared to group IIb, *: significant compared to group IIIa, #: significant compared to group IIIb. One-way ANOVA followed by Turkey's post-hoc test

DISCUSSION

DOX-induced model of nephropathy has been commonly used[28]. Interestingly, CeO2NPs represent a powerful antioxidant[13]. Quercetin is a flavonoid present in food and has anti-inflammatory effects[29].

In our study to induce an animal model of nephropathy, we injected rats with six equal doses of DOX intraperitoneally for 14 days with a total cumulative dose of 15 mg/kg. This work aimed to compare the possible therapeutic effect of CeO2NPs and quercetin on DOX-induced nephropathy at different time points.

Our study revealed that the body and kidney weight coefficient significantly decreased in groups IIa and IIb compared to controls in a duration-dependent manner with group IIb significantly more affected as compared to group IIa, due to DOX-induced loss of appetite, and malabsorption due to intestinal injury. In line with our results were the findings of Shati and El-Kott[30].

In our experiment, we found significantly elevated serum urea, creatinine, cholesterol, and triglyceride in DOX-treated groups while significantly decreased serum albumin, and HDL concentration compared to control in duration dependent manner with group IIb significantly more affected as compared to group IIa. This agrees with Afsar *et al*.[31] and Fan *et al*.[32]. This might be due to the destruction of the glomerular filtration barrier causing hypoalbuminemia. DOX stimulated lipogenesis in the liver leading to hyperlipidemia. In addition. DOX led to a disturbance in fat metabolism[4].

DOX-induced nephropathy is characterized by decreased serum albumin due to proteinuria and increased serum levels of urea and creatinine, all of which are attributed to DOX-induced renal toxicity caused by oxidative stress and inflammatory condition[4].

DOX-induced nephropathy was progressive with increased duration after injection was stopped because DOX is rapidly cleared from the plasma after administration, deposited in tissues mainly the kidneys, and slowly excreted into the urine[33].

Histological changes in our study were observed both in glomeruli and tubules. Glomerular changes were in the form of widening of urinary space, and congested glomerular capillaries. Moreover, renal tubular degenerative changes in the form of vacuolated cytoplasm and deeply stained pyknotic nuclei were observed. Proximal renal tubules had degenerated brush borders. These changes were progressive with the increased duration after DOX injection was stopped; they were more obvious in group IIb.

This agrees with Al-Hassawi and Al-Sammak[34] and Mahmoud *et al*.[35]. According to Al-Hassawi and Al-Sammak[34], dilation of Bowman's capsule after DOX administration was due to vasoconstriction in the blood vessels as a protective mechanism from cell damage. This induced glomerular atrophy and widening of the urinary space. According to Shati and El-Kott[30], the mechanism by which DOX induces renal pathology may be an excess production of ROS due to the depletion of antioxidants, mitochondrial dysfunction, and iron-dependent apoptosis. In addition, apoptotic cell death due to increased free radicals led to lipid peroxidation and subsequent cell membrane disruption resulting in cell death[36]. In addition, Hozayen *et al*.[37] reported that DOX tended to accumulate in mitochondria leading to mitochondrial dysfunction.

We observed also tubular dilatation and intraluminal acidophilic casts in renal tubules. Our results agreed with Zickri *et al*.[38], Sadek *et al*.[39], and El-Sheikh *et al*.[40]. Cast formation could be attributed to the glomerular filtration barrier dysfunction caused by DOX-induced

podocyte injury which allowed the passage of proteins in the tubules. Protein accumulation intraluminal led to protein cast formation. Casts obstruct renal tubules with subsequent increased intratubular pressure and dilation of the lumen[41]. Also, these proteins induce tubular epithelium injury[42]. According to Zickri *et al*.[38], DOX-induced tubular epithelium desquamation into the lumen is a result of the damage to the cell membrane induced by lipid peroxidation.

In the present study, we found interstitial inflammatory cellular infiltration in renal tissue which could be explained by the presence of free radicals which induce an inflammatory response and trigger the release of interleukin-1[43]. Similar to our results, Abd-Ellatif *et al*.[44] found that the inflammatory response led to glomerular congestion, which decrease the ability to clear toxic radicals.

In our results, PAS revealed that the basement membranes increased in thickness in DOX-treated groups with a significant increase in PAS area percentage compared to the control groups. These changes were significantly more in group IIb versus group IIa. Similar results were previously reported by Sang *et al*.[45], due to increased extracellular matrix deposition in basement membranes and mesangial matrix in response to injury.

The brush borders of the proximal tubules appeared irregular and interrupted by PAS which confirmed H&E finding. Similarly, Sadek *et al*.[39] found disruption of brush borders in most tubules but with the interruption of basal laminae. They clarified that DOX-induced pathology resulted in damage to the cytoskeleton, which led to the destruction of microvilli, and cell junctions.

In our study, we found significantly increased collagen fibers with interstitial fibrosis in DOX-induced nephropathy which was more prominent with longer duration in group IIb. This was in line with the results of Sadek *et al*.[39] and Shati and El-Kott[30]. DOX-induced renal interstitial fibrosis could be attributed to the DOX-induced tubulointerstitial inflammation with subsequent secretion of transforming growth factor-beta (TGF-β) which stimulates myofibroblasts to increase deposition of extracellular matrix[39,46]. The fibrosis observed in our results in DOX nephropathy was progressive with increased duration due to sustained inflammation induced by DOX accumulation in renal tissue. The intensity of inflammation correlated with induced renal fibrosis[42].

A significant duration-dependent increase in PCNA positive cells was detected in our results in the DOX nephropathy groups; being significantly higher in group IIb versus IIa. Our results were in line with those of Han *et al*.[47] who reported that the incidence of tubular cell division increases in stress conditions. In addition, Sakr and Abo-El-Yazid[48] reported increased PCNA expression in DOX-induced hepatotoxicity in a duration-dependent manner.

PCNA has an important role in controlling DNA synthesis as well as cell proliferation. PCNA expression increase at the end of the G1 phase reached its maximum in the S phase[49]. PCNA is an essential component of DNA replication, representing the processing factor for DNA polymerases. Although DOX treatment inhibits cell proliferation in cancer cells through cell cycle arrest at the G2/M phase[50], it was found that DOX significantly increased cell entry to the S phase in non-cancer cells as a compensatory response to cell injury[51]. This explains the DOX-induced increase in PCNA expression in our results. In addition to its role in replication, PCNA is needed during DNA repair after cell damage through nucleotide excision[52].

In the present study, a significant increase in AFP expression was observed in the DOX groups. This was explained by the sustained inflammation induced in DOX-treated groups in our study. Mizejewski[53] reported that AFP was able to induce an inflammatory response via binding to arachidonic acids. It regulated the transfer of arachidonic acid into cells, probably through specific cell surface AFP receptors.

In addition, it was found that alpha-fetoprotein is expressed in the fetal liver and to a lesser extent in the gut and kidney. However, AFP proceeds to function as a negative acute phase protein in adults and is expressed in cases of liver cancer[54]. AFP is exclusively synthesized by the liver in adult but it might be induced in renal injury as a stress response[55]. AFP activates the cAMP protein kinase-A pathway and induces Ca2+ influx, which enhances DNA synthesis and cell proliferation[56]. This explained that the DOX-induced increased AFP expression in our study was due to cell proliferation in response to cell damage.

In the current work, WT-1 positive podocytes significantly decreased in DOX nephropathy groups. These results agreed with previous studies[47,57]. Wu *et al*.[46] used WT-1 as a marker of podocyte which was downregulated in podocyte injury. In addition, an association was found between WT-1 mutation and an immune complex-related membranoproliferative glomerulonephritis in a previous study[58]. This was explained by Bryant *et al*.[57] who found that WT-1 is a transcriptional master regulator of podocyte differentiation and function acting on podocyte-specific target genes such as nephrin genes. Podocytes play a key role in glomerular filtration. Injury to podocytes can disrupt slit diaphragm structure and impair its function, leading to proteinuria and subsequent hypoalbuminemia[59]. This confirms our previous biochemical and histological results.

Ultrastructural findings also confirmed our previous results. We found tubular degenerative changes by electron microscope in the form of ill-defined basal infoldings with a heterochromatic nucleus, irregular nuclear membrane, clumps of peripheral heterochromatin, and destructed brush borders. These results were in agreement with Alagal *et al*.[60] and Kandil *et al*.[61]. This might be explained by the

nuclear damage which occurred because DOX inhibited both DNA polymerase and topoisomerase II responsible for DNA cleavage and duplication which led to nuclear damage[61]. Apoptotic changes could be attributed to oxidative stress[60].

In the current work, an irregular thickness of GBM and effacement of foot processes of podocyte were observed by electron microscopy in DOX-treated groups which were more prominent with increased duration of stopping DOX. This was in agreement with the results of Na *et al*.[62] and Ma *et al*.[63]. Massive podocyte fusion was seen because DOX caused podocyte injury via the downregulation of podocin which suppressed slit diaphragm formation[54].

Administration of CeO2NPs to DOX nephropathy restored body weight and relative kidney weight, improved renal functions; decreased blood urea and creatinine, and alleviated hyperlipidemia. Bashandy *et al*.[64] reported similar results and explained that by the improved renal structural changes. Its antioxidant role could be attributed to the structure of the cerium atom in the form of a crystal lattice. Cerium redox reacts on the surface of the formed nanoparticles[65]. Moreover, Carvajal ***et al***.[66] reported an anti-lipogenic effect of CeO2NPs in a model of fatty liver which could explain the improvement of hyperlipidemia in our model.

In groups IIIa and IIIb, the administration of CeO2NPs to DOX nephropathy alleviated toxic and degenerative changes produced by DOX in the glomeruli and tubules both in the short and long durations of DOX cessation. CeO2NPs could be uptaken by cells via endocytosis, and then distributed in the cytoplasm without passing into the nucleus. Thus, they could reduce intracellular ROS and maintain the normal functions of mitochondria[67] which were impaired by DOX. Also, CeO2NPs act as nitric oxide scavengers and have superoxide dismutase mimetic activity[68].

Similar results were reported by Hamad[65]. In addition, Jahani *et al*.[69] reported an antioxidant role of CeO2NPs activity in animal models of diabetic nephropathy. CeO2NPs had anti-inflammatory and anti-apoptotic properties[13]. Hamzeh *et al*.[70] proved the protective effect of CeO2NPs against testicular toxicity induced by cyclophosphamide via antioxidant and anti-apoptotic roles with downregulation of caspase-3. CeO2NPs could prevent retinal degeneration induced by hydrogen peroxide molecules[71]. Similarly, it was previously reported that CeO2NPs could inhibit apoptosis in mouse bone marrow stromal cells via their antioxidant role in a dose-dependent manner[67].

The CeO2NPs ability to relieve inflammatory cell aggregation induced in DOX nephropathy could be attributed to their anti-inflammatory properties. Similar results were reported by Hamad and Hamad[72] in a model of monosodium glutamate-induced renal injury.

In the current work, PAS percentage area significantly decreased in groups IIIa and IIIb versus DOX-treated groups of the same duration which indicates a reduction of the increased extracellular matrix deposition in basement membranes induced by DOX. Also, attenuation of brush border interruption in the proximal tubules was observed. Similarly, Hamzeh *et al*.[73] reported that CeO2NPs attenuated the increased PAS area percentage in cyclophosphamide-induced renal toxicity in mice. Saleh *et al*.[74] reported similar results in the toxicity of the epididymis with the restoration of stereocilia.

In the present study, CeO2NPs alleviated collagen fibers deposition. Similarly, Saifi *et al*.[75] reported that CeO2NPs alleviated renal fibrosis by inhibiting TGF-β signaling. In addition, Oró *et al*.[9] reported an antifibrotic effect of CeO2NPs in a rat model of hepatic fibrosis

The alleviation of functional and structural manifestations of nephropathy could be attributed to that CeO2NPs reversed podocyte injury as indicated by restoring the down-regulated expression of WT-1 and the euchromatic nucleus of podocyte and decreased effacement in the ultrastructure. Also, the reduction of PCNA and AFP expression indicates the decrease in cell proliferation which was induced by DOX toxicity.

In contrast, CeO2NPs were toxic to lung fibroblasts in a culture which could be attributed to the different media conditions[76]. Moreover, different effects of CeO2NPs are related to differences in diameter, shape, preparation method, and surface charges during the synthesis of the nanoparticles[77].

In groups IVa and IVb, administration of quercetin to the DOX model of nephropathy restored body weight and relative kidney weight, improved renal functions, and alleviated hyperlipidemia. Also, it reduced histopathological and ultrastructural changes produced by DOX but to a less extent versus CeO2NPs. Heeba and Mahmoud[14] explained that it has potent antioxidant and anti-apoptotic effects by suppressing the overexpression of inducible nitric oxide synthase. The degenerative changes were attenuated by quercetin because its precursor, rutin, could attenuate renal tubular cell apoptosis via the downregulation of caspase3,7[78]. In addition, Talirevic and Jelena[79] reported the role of quercetin in the treatment of dyslipidemia.

Quercetin attenuated DOX-induced renal interstitial inflammatory infiltration due to its anti-inflammatory role as reported by Ren *et al*.[80].

Similar to our results, Moustafa and Ali[81] found that quercetin improved DOX-induced oxidative stress in the liver. In addition, Hashish *et al*.[82] found that quercetin attenuated DOX-induced cardiotoxicity.

We observed PAS percentage area reduction in groups IVa and IVb versus DOX-treated groups of the same duration. This was because quercetin inhibited extracellular matrix deposition induced by tissue injury. Similar results

were observed by Ren *et al*.[80]. PAS demonstrated partial restoration of the brush border after quercetin administration which was confirmed by the electron microscope. Similar results were reported by Alshammari *et al*.[12] in a model of cadmium chloride-induced renal toxicity and they attributed this to its antioxidant effect.

Quercetin attenuated DOX-induced renal interstitial fibrosis. Similar results were observed by Widowati *et al*.[83] and Ren *et al*.[80]. They explained that the antifibrotic effect of quercetin was via downregulation of TGF-β and suppression of myofibroblast activation.

Quercetin attenuated the increased PCNA and AFP expression due to its antioxidant role which suppressed tissue injury. Quercetin alleviated podocyte injury as demonstrated by the restoration of WT-1 expression and ultrastructurally. Thus, quercetin could suppress proteinuria. Similar results were reported by Liu *et al*.[84].

In contrast to our results, Rangan *et al*.[85] reported that quercetin did not improve DOX-induced nephropathy. It did not downregulate Nuclear Factor-κB, and this could in part explain the lower effect exhibited by quercetin versus CeO2NPs in the improvement of nephropathy.

Interestingly, group V showed a progressive increase in DOX-induced degenerative changes. Marked irregular thickening in the GBM with tubular dilatation and tubular epithelial desquamation were seen. Tubular casts were obvious. Suppressed WT-1 expression and increased AFP and PCNA positive cells were detected. These findings indicated the progression of nephropathy and that this model is irreversible. On the other hand, this confirmed the therapeutic role exerted by CeO2NPs and quercetin which were administrated for a similar duration. Similar results were reported byTabatabaeifar *et al*.[86]. In addition, they found a progressive decrease in WT-1 mRNA expression. This progressive course after stopping the injection of DOX could be attributed to its tendency to accumulate in kidney tissue[87].

CONCLUSION

DOX caused duration-dependent renal toxicity. CeO2NPs were more effective compared to quercetin in attenuating renal degenerative changes, reversing podocyte injury, and decreasing fibrosis in the DOX-induced rat model of nephropathy.

ABBREVIATIONS

CeO2NPs: Cerium oxide nanoparticles; **DOX:** doxorubicin; **PCNA:** proliferating cell nuclear antigen; **AFP:** alpha-fetoprotein; **WT-1:** Wilms tumor-1; **TGF-β:** transforming growth factor-β.

CONFLICT OF INTERESTS

There are no conflicts of interest.

REFERENCES

1. Wen, C., Fu, L., Huang, J., Dai, Y., Wang, B., Xu, G., Wu, L., and Zhou, H. Curcumin reverses doxorubicin resistance via inhibition the efflux function of ABCB4 in doxorubicin-resistant breast cancer cells. Molecular medicine reports. 2019; 19(6): p. 5162-5168. DOI. DOI: 10.3892/mmr.2019.10180
2. Renu, K., Pureti, L.P., Vellingiri, B., and Valsala Gopalakrishnan, A. Toxic effects and molecular mechanism of doxorubicin on different organs–an update. Toxin Reviews. 2022; 41(2):p.650-674.DOI. https://www.tandfonline.com/action/showCitFormats?doi=10.1080/15569543.2021.1912099
3. Fan, H.-y., Wang, X.-k., Li, X., Ji, K., Du, S.-h., Liu, Y., Kong, L.-l., Xu, J.-c., Yang, G.-q., and Chen, D.-q. Curcumin, as a pleiotropic agent, improves doxorubicin-induced nephrotic syndrome in rats. J. Ethnopharmacol. 2020; 250: p. 112502. DOI.:10.1016/j.jep.2019.112502
4. Soltani Hekmat, A., Chenari, A., Alipanah, H., and Javanmardi, K. Protective effect of alamandine on doxorubicin-induced nephrotoxicity in rats. BMC Pharmacology and Toxicology. 2021; 22(1): p. 31. DOI: 10.1186/s40360-021-00494-x.
5. Singh, K.R., Nayak, V., Sarkar, T., and Singh, R.P. Cerium oxide nanoparticles: properties, biosynthesis and biomedical application. RSC advances. 2020; 10(45): p. 27194-27214. DOI. https://doi.org/10.1039/D0RA04736H
6. Nadeem, M., Khan, R., Afridi, K., Nadhman, A., Ullah, S., Faisal, S., Mabood, Z.U., Hano, C., and Abbasi, B.H. Green synthesis of cerium oxide nanoparticles (CeO2 NPs) and their antimicrobial applications: a review. International journal of nanomedicine. 2020; 15: p. 5951. DOI. https://doi.org/10.2147/IJN.S255784
7. Bashandy, S.A., Abdelhameed, M.F., and Ahmed-Farid, O.A. The Pivotal role of Cerium oxide nanoparticles in thioacetamide induced hepatorenal injury in rat. Egyptian journal of chemistry. 2022; 65(10): p. 267-278. DOI. https://doi.org/10.21608/ejchem.2022.115482.5242
8. Jahani, M., Shokrzade, M., Vafaei-Pour, Z., Zamani, E., and Shaki, F. Potential Role of Cerium Oxide Nanoparticles for Attenuation of Diabetic Nephropathy by Inhibition of Oxidative Damage. Asian Journal of Animal and Veterinary Advances. 2016; 11: p. 226-234. DOI: 10.3923/ajava.2016.226.234.
9. Oró, D., Yudina, T., Fernández-Varo, G., Casals, E., Reichenbach, V., Casals, G., de la Presa, B.G., Sandalinas, S., Carvajal, S., and Puntes, V. Cerium oxide nanoparticles reduce steatosis, portal hypertension and display anti-inflammatory properties in rats with liver fibrosis. Journal of hepatology. 2016; 64(3): p. 691-698. DOI. https://doi.org/10.1016/j.jhep.2015.10.020

10. Deepak, M., Sulaiman, C., Balachandran, I., and Chandran, K. Anti-oxidant, anti-proliferative activities and characterization of secondary metabolites using Q-TOF-LC-MS/MS analysis of anti-aging medicinal plant Holostemma ada-kodien. Vegetos. 2022: p. 1-10. DOI. https://doi.org/10.1007/s42535-022-00529-6
11. Tu, H., Ma, D., Luo, Y., Tang, S., Li, Y., Chen, G., Wang, L., Hou, Z., Shen, C., and Lu, H. Quercetin alleviates chronic renal failure by targeting the PI3k/Akt pathway. Bioengineered. 2021; 12(1):p.6538-6558.DOI. https://doi.org/10.1080/21655979.2021.1973877
12. Alshammari, G.M., Al-Qahtani, W.H., AlFaris, N.A., Albekairi, N.A., Alqahtani, S., Eid, R., Yagoub, A.E.A., Al-Harbi, L.N., and Yahya, M.A. Quercetin alleviates cadmium chloride-induced renal damage in rats by suppressing endoplasmic reticulum stress through SIRT1-dependent deacetylation of Xbp-1s and eIF2α. Biomedicine & Pharmacotherapy. 2021; 141: p. 111862. DOI: https://doi.org/10.1016/j.biopha.2021.111862.
13. Ibrahim, H.G., Attia, N., Fatma El Zahraa, A.H., El Heneidy, M.A.J.B., and Pharmacotherapy. Cerium oxide nanoparticles: In pursuit of liver protection against doxorubicin-induced injury in rats. 2018;103:p.773-781.DOI. https://doi.org/10.1016/j.biopha.2018.04.075
14. Heeba, G.H. and Mahmoud, M.E. Dual effects of quercetin in doxorubicin-induced nephrotoxicity in rats and its modulation of the cytotoxic activity of doxorubicin on human carcinoma cells. Environmental toxicology. 2016; 31(5): p. 624-36. DOI: 10.1002/tox.22075.
15. Ali, E., El Fiky, S., El-Batsh, M., El-Dien, M., and Safan, M. The protective effect of metformin and exenatide on doxorubicin-induced nephrotoxicity in rats. Menoufia Medical Journal. 2021; 34(3): p. 1060-1067. DOI: 10.4103/mmj.mmj_217_20.
16. Internet Addiction: The Emergence of a New Clinical Disorder. CyberPsychology & Behavior. 1998; 1(3): p. 237-244. DOI: 10.1089/cpb.1998.1.237.
17. Porwal, M., Khan, N.A., and Maheshwari, K.K. Evaluation of acute and subacute oral toxicity induced by ethanolic extract of Marsdenia tenacissima leaves in experimental rats. Scientia Pharmaceutica. 2017; 85(3): p. 29. DOI. https://doi.org/10.3390/scipharm85030029
18. Tabacco, A., Meiattini, F., Moda, E., and Tarli, P. Simplified enzymic/colorimetric serum urea nitrogen determination. Clinical chemistry. 1979; 25(2): p. 336-337.
19. Fabiny, D.L. and Ertingshausen, G. Automated reaction-rate method for determination of serum creatinine with the CentrifiChem. Clinical chemistry. 1971; 17(8): p. 696-700. DOI. https://doi.org/10.1093/clinchem/17.8.696
20. Bancroft, J.D. and Layton, C. Histological Techniques in Bancroft's Theory and Practice of Histological Techniques. seventh ed., ed. S.K. Suvarna, C. Layton, and J.D. Bancroft. 2013, Oxford: Churchill Livingstone.173-186.
21. Mohamed, H.K. and Meligy, F.Y. The possible protective Effects of Alfa Lipoic Acid on Diethanolamine-Induced Renal Toxicity in Adult Male Albino Rats: A Histological and Immunohistochemical Study. Egyptian Journal of Histology. 2018; 41(4): p. 431-444. DOI: 10.21608/ejh.2018.3929.1010.
22. Lavres Junior, J., Reis, A.R., Rossi, M.L., Cabral, C.P., Nogueira, N.d.L., and Malavolta, E. Changes in the ultrastructure of soybean cultivars in response to manganese supply in solution culture. Scientia Agricola. 2010; 67(3): p. 287-294. DOI: DOI: 10.1590/S0103-90162010000300006.
23. Yang, X., Han, X., Wen, Q., Qiu, X., Deng, H., and Chen, Q. Protective Effect of Keluoxin against Diabetic Nephropathy in Type 2 Diabetic Mellitus Models. Evidence-Based Complementary and Alternative Medicine. 2021; 2021: p. 8455709. DOI: 10.1155/2021/8455709.
24. Bohuslavova, R., Cerychova, R., Nepomucka, K., and Pavlinkova, G. Renal injury is accelerated by global hypoxia-inducible factor 1 alpha deficiency in a mouse model of STZ-induced diabetes. BMC endocrine disorders. 2017; 17(1): p. 1-12. DOI. https://doi.org/10.1186/s12902-017-0200-8
25. Chaloob, M., Ali, H., Qasim, B., and Mohammed, A. Immunohistochemical Expression of Ki-67, PCNA and CD34 in Astrocytomas: A Clinicopathological Study. Oman medical journal. 2012; 27: p. 368-74. DOI: 10.5001/omj.2012.93.
26. Tomita, N., Hotta, Y., Naiki-Ito, A., Sanagawa, A., Kataoka, T., Furukawa-Hibi, Y., Takahashi, S., and Kimura, K. Protective effects of tadalafil on damaged podocytes in an adriamycin-induced nephrotic syndrome model. Journal of Pharmacological Sciences. 2022; 149(2): p. 53-59. DOI: https://doi.org/10.1016/j.jphs.2022.03.003.
27. Bryman, A. and Cramer, D.Quantitative data analysis with SPSS 14, 15 & 16: A guide for social scientists. in Quantitative data analysis with SPSS 14, 15 & 16: A guide for social scientists. 2009, New York, NY, US: Routledge/Taylor & Francis Groupxxv, 381-xxv, 381.
28. Pereira, W.d.F., Brito-Melo, G.E.A., de Almeida, C.A.S., Moreira, L.L., Cordeiro, C.W., Carvalho, T.G.R., Mateo, E.C., and Simoes e Silva, A.C. The experimental model of nephrotic syndrome induced by Doxorubicin in rodents: an update. Journal of Inflammation Research. 2015; 64(5): p. 287-301. DOI. https://doi.org/10.1007/s00011-015-0813-1

29. Nazmi, A.S., Ahmad, S.J., Pillai, K.K., Akhtar, M., Ahmad, A., and Najmi, A.K. Protective effects of Bombyx mori, quercetin and benazepril against doxorubicin induced cardiotoxicity and nephrotoxicity. Journal of Saudi Chemical Society. 2016; 20: p. S573-S578. DOI. https://doi.org/10.1016/j.jscs.2013.04.001

30. Shati, A.A. and El-Kott, A.F. Acylated ghrelin protects against doxorubicin-induced nephropathy by activating silent information regulator 1. Basic and Clinical Pharmacology and Toxicology 2021; 128(6): p. 805-821. DOI. https://doi.org/10.1111/bcpt.13569

31. Afsar, T., Razak, S., Almajwal, A., and Aldisi, D. Doxorubicin-induced alterations in kidney functioning, oxidative stress, DNA damage, and renal tissue morphology; Improvement by Acacia hydaspica tannin-rich ethyl acetate fraction. Saudi Journal of Biological Sciences. 2020; 27(9): p. 2251–2260. DOI: 10.1016/j.sjbs.2020.07.011.

32. Fan, H., Yang, M., Qi, D., Zhang, Z., Zhu, L., Shang-Guan, X.-X., Liu, K., Xu, H., and Che, X. Salvianolic acid A as a multifunctional agent ameliorates doxorubicin-induced nephropathy in rats. J Scientific Reports. 2015; 5: p. 9-15. DOI.

33. LEE, V.W. and HARRIS, D.C. Adriamycin nephropathy: A model of focal segmental glomerulosclerosis. Nephrology. 2011; 16(1): p. 30-38. DOI: https://doi.org/10.1111/j.1440-1797.2010.01383.x.

34. Al-Hassawi, W.W. and Al-Sammak, M.A. Effect of doxorubicin on the histological structure of the kidneys in male albino rats. Journal of the Faculty of Medicine Baghdad. 2013; 55(4): p. 384-389. DOI. https://doi.org/10.32007/jfacmedbagdad.554595

35. Mahmoud, H., Ahmed, O., Fahim, H., Ahmed, N., and Ashour, M.J.A.A.V.S. Effects of rutin and quercetin on doxorubicin-induced renocardiotoxicity in male wistar rats. Advances in Animal and Veterinary Sciences. 2020; 8(4): p. 370-384. DOI. http://dx.doi.org/10.17582/journal.aavs/2020/8.4.370.384

36. Hirst, S.M., Karakoti, A.S., Tyler, R.D., Sriranganathan, N., Seal, S., and Reilly, C.M. Anti-inflammatory properties of cerium oxide nanoparticles. Small. 2009; 5(24): p. 2848-2856. DOI. https://doi.org/10.1002/smll.200901048

37. Hozayen, W.G., Abou Seif, H.S., and Amin, S. Protective effects of ruitn and/or hesperidin against doxorubicin-induced hepatotoxicity. International Journal of Clinical Nutrition. 2014; 2(1): p. 11-7. DOI.:10.12691/ijcn-2-1-2

38. Zickri, M.B., Zaghloul, S., Farouk, M., and Abdel Fattah, M.M.A. Effect of stem cell therapy on adriamycin induced tubulointerstitial injury. International journal of stem cells. 2012; 5(2): p. 130. DOI. https://doi.org/10.15283%2Fijsc.2012.5.2.130

39. Sadek, E.M., Salama, N.M., Ismail, D.I., and Elshafei, A.A. Histological study on the protective effect of endogenous stem-cell mobilization in Adriamycin-induced chronic nephropathy in rats. Journal of microscopy and ultrastructure. 2016; 4(3): p. 133-142. DOI. https://doi.org/10.1016/j.jmau.2015.12.003

40. El-Sheikh, A.A., Morsy, M.A., Mahmoud, M.M., Rifaai, R.A., and Abdelrahman, A.M. Effect of coenzyme-Q10 on doxorubicin-induced nephrotoxicity in rats. J Advances in pharmacological sciences. 2012; 2012: p. e981461. DOI. https://doi.org/10.1155/2012/981461

41. Allahyari, M., Samadi-Noshahr, Z., Hosseinian, S., Salmani, H., Noras, M., and Khajavi-Rad, A. Camel milk and allopurinol attenuated adenine-induced acute renal failure in rats. Iranian Journal of Science and Technology, Transactions A: Science. 2021; 45(5): p. 1539-1548. DOI. https://doi.org/10.1007/s40995-021-01155-8

42. Szalay, C.I., Erdélyi, K., Kökény, G., Lajtár, E., Godó, M., Révész, C., Kaucsár, T., Kiss, N., Sárközy, M., Csont, T., Krenács, T., Szénási, G., Pacher, P., and Hamar, P. Oxidative/Nitrative Stress and Inflammation Drive Progression of Doxorubicin-Induced Renal Fibrosis in Rats as Revealed by Comparing a Normal and a Fibrosis-Resistant Rat Strain. PloS one. 2015; 10(6): p. e0127090. DOI: 10.1371/journal.pone.0127090. https://doi.org/10.1371/journal.pone.0127090

43. Rafiee, Z., Moaiedi, M.Z., Gorji, A.V., and Mansouri, E. p-Coumaric acid mitigates doxorubicin-induced nephrotoxicity through suppression of oxidative stress, inflammation and apoptosis. J Archives of Medical Research 2020; 51(1): p. 32-40. DOI. https://doi.org/10.1016/j.arcmed.2019.12.004

44. Abd-Ellatif, R.N., Nasef, N.A., El-Horany, H.E.-S., Emam, M.N., Younis, R.L., Gheit, E., Abo, R.E., Elseady, W., Radwan, D.A., and Hafez, Y.M. Adrenomedullin Mitigates Doxorubicin-Induced Nephrotoxicity in Rats: Role of Oxidative Stress, Inflammation, Apoptosis, and Pyroptosis. Int. J. Mol. Sci. 2022; 23(23): p. 14570. DOI. https://doi.org/10.3390/ijms232314570

45. Sang, Y., Tsuji, K., Inoue-Torii, A., Fukushima, K., Kitamura, S., and Wada, J. Semaphorin3A-Inhibitor Ameliorates Doxorubicin-Induced Podocyte Injury. Int. J. Mol. Sci. 2020; 21(11). DOI: 10.3390/ijms21114099.

46. Wu, Q., Li, W., Zhao, J., Sun, W., Yang, Q., Chen, C., Xia, P., Zhu, J., Zhou, Y., Huang, G., Yong, C., Zheng, M., Zhou, E., and Gao, K. Apigenin ameliorates doxorubicin-induced renal injury via inhibition of oxidative stress and inflammation. Biomedicine & Pharmacotherapy. 2021; 137: p. 111308. DOI: https://doi.org/10.1016/j.biopha.2021.111308.

47. Han, P., Cai, Y., Wang, Y., Weng, W., Chen, Y., Wang, M., Zhan, H., Yu, X., Wang, T., and Shao, M. Artemether ameliorates kidney injury by restoring redox imbalance and improving mitochondrial function in Adriamycin nephropathy in mice. J Scientific reports. 2021; 11(1): p. 1-14. DOI. https://doi.org/10.1038/s41598-020-80298-x

48. Sakr, S.A. and Abo-El-Yazid, S.M. Effect of fenugreek seed extract on adriamycin-induced hepatotoxicity and oxidative stress in albino rats. Toxicol. Ind. Health. 2012; 28(10): p. 876-85. DOI: 10.1177/0748233711425076.

49. A, P., Xu, X., Wang, C., Yang, J., Wang, S., Dai, J., and Ye, L. EZH2 promotes DNA replication by stabilizing interaction of POLδ and PCNA via methylation-mediated PCNA trimerization. Epigenetics & Chromatin. 2018; 11(1): p. e44. DOI: 10.1186/s13072-018-0213-1.

50. Mansilla, S.F., De La Vega, M.B., Calzetta, N.L., Siri, S.O., and Gottifredi, V. CDK-Independent and PCNA-Dependent Functions of p21 in DNA Replication. Genes. 2020; 11(6): p. e593. DOI. https://doi.org/10.3390/genes11060593

51. Xie, K., Xu, C., Zhang, M., Wang, M., Min, L., Qian, C., Wang, Q., Ni, Z., Mou, S., Dai, H., and Disease. Yes-associated protein regulates podocyte cell cycle re-entry and dedifferentiation in adriamycin-induced nephropathy. J Cell Death. 2019; 10(12): p. 1-15. DOI. https://doi.org/10.1038/s41419-019-2139-3

52. Zheng, F., Georgescu, R., Yao, N.Y., Li, H., and O'Donnell, M.E. Cryo-EM structures reveal that RFC recognizes both the 3'- and 5'-DNA ends to load PCNA onto gaps for DNA repair. eLife. 2022; 11. DOI: 10.7554/eLife.77469.

53. Mizejewski, G. Alpha-fetoprotein (AFP) and inflammation: Is AFP an Acute and/or Chronic Phase Reactant. Pathophysiology of Haemostasis and Thrombosis. 2015; 3: p. e191. DOI. http://dx.doi.org/10.4172/2329-8790.1000191

54. Ahmed, O.M., Galaly, S.R., Mostafa, M.M.A., Eed, E.M., Ali, T.M., Fahmy, A.M., and Zaky, M.Y. Thyme Oil and Thymol Counter Doxorubicin-Induced Hepatotoxicity via Modulation of Inflammation, Apoptosis, and Oxidative Stress. Oxidative Medicine and Cellular Longevity. 2022; 2022: p. e6702773. DOI: 10.1155/2022/6702773.

55. Zager, R.A., Vijayan, A., and Johnson, A.C. Proximal tubule haptoglobin gene activation is an integral component of the acute kidney injury "stress response". American journal of physiology. Renal physiology. 2012; 303(1): p. F139-48. DOI: 10.1152/ajprenal.00168.2012.

56. Lin, B., Wang, Q., Liu, K., Dong, X., Zhu, M., and Li, M. Alpha-Fetoprotein Binding Mucin and Scavenger Receptors: An Available Bio-Target for Treating Cancer. Front. Oncol. 2021; 11: p. 625936. DOI: 10.3389/fonc.2021.625936.

57. Bryant, C., Cianciolo, R., Govindarajan, R., and Agrawal, S. Adriamycin-Induced Nephropathy is Robust in N and Modest in J Substrain of C57BL/6. Frontiers in cell and developmental biology. 2022; 10: p. e924751. DOI: 10.3389/fcell.2022.924751.

58. Anderson, E., Aldridge, M., Turner, R., Harraway, J., McManus, S., Stewart, A., Borzi, P., Trnka, P., Burke, J., and Coman, D. WT1 complete gonadal dysgenesis with membranoproliferative glomerulonephritis: case series and literature review. Pediatric nephrology (Berlin, Germany). 2022; 37(10): p. 2369-2374. DOI: 10.1007/s00467-022-05421-8.

59. Liu, S., Jia, Z., Zhou, L., Liu, Y., Ling, H., Zhou, S.-F., Zhang, A., Du, Y., Guan, G., and Yang, T. Nitro-oleic acid protects against adriamycin-induced nephropathy in mice. American journal of physiology. Renal physiology. 2013; 305(11): p. F1533-F1541. DOI: 10.1152/ajprenal.00656.2012.

60. Alagal, R.I., AlFaris, N.A., Alshammari, G.M., ALTamimi, J.Z., AlMousa, L.A., and Yahya, M.A. Kaempferol attenuates doxorubicin-mediated nephropathy in rats by activating SIRT1 signaling. Journal of Functional Foods. 2022; 89: p. 104918. DOI. https://doi.org/10.1016/j.jff.2021.104918

61. Kandil, E.H., Okdah, Y.A., and Moselhy, A.G. Histological, ultrastructural, and biochemical studies on the expected role of thyme oil on ameliorating renal toxicity induced by doxorubicin in female albino rats. The Egyptian Society of Experimental Biology. 2022; 18(1): p. 91-100. DOI. 10.5455/egysebz.20220507065051

62. Na, W., Ri-Bao, W., Qing-Ping, L., Xi, Y., and Xiang-Mei, C. Protective effects of astragaloside in rats with adriamycin nephropathy and underlying mechanism. Chinese journal of natural medicines. 2016; 14(4): p. 270-277. DOI. https://doi.org/10.1016/S1875-5364(16)30027-9

63. Ma, H., Wu, Y., Zhang, W., Dai, Y., Li, F., Xu, Y., Wang, Y., Tu, H., Li, W., and Zhang, X. The effect of mesenchymal stromal cells on doxorubicin-induced nephropathy in rats. Journal of Cytotherapy. 2013; 15(6): p. 703-711. DOI. https://doi.org/10.1016/j.jcyt.2013.02.002

64. Bashandy, M., Saeed, H., Ahmed, W., Ibrahim, M., and Shehata, O. Ameliorative Effect of Cerium Oxide Nanoparticles against Cadmium Nephrotoxicity in Male Albino Rats. Journal of Veterinary Medical Research. 2021; 28(2): p. 62-75. DOI. https://dx.doi.org/10.21608/jvmr.2021.105032.1045

65. Hamad, S.R. Cardio-Renal Protective Role of Cerium Oxide Nanoparticle in Preventing Histopathological Lesions, and Collagen Deposition Produced From Lead Acetate Injection in *Vivo*: Light Microscopic Examination. Egyptian Journal of Histology. 2022; 45(3): p. 815-824. DOI: 10.21608/ejh.2021.73043.1466.

66. Carvajal, S., Perramón, M., Oró, D., Casals, E., Fernández-Varo, G., Casals, G., Parra, M., González de la Presa, B., Ribera, J., Pastor, Ó., Morales-Ruíz, M., Puntes, V., and Jiménez, W. Cerium oxide nanoparticles display antilipogenic effect in rats with non-alcoholic fatty liver disease. Scientific reports. 2019; 9(1): p. e12848. DOI: 10.1038/s41598-019-49262-2.

67. Zhang, Q., Ge, K., Duan, J., Chen, S., Zhang, R., Zhang, C., Wang, S., and Zhang, J. Cerium oxide nanoparticles protect primary mouse bone marrow stromal cells from apoptosis induced by oxidative stress. Journal of Nanoparticle Research. 2014; 16: p. e2697. DOI: 10.1007/s11051-014-2697-3.

68. Elshony, N., Nassar, A.M.K., El-Sayed, Y.S., Samak, D., Noreldin, A., Wasef, L., Saleh, H., Elewa, Y.H.A., Tawfeek, S.E., Saati, A.A., Batiha, G.E., Tomczyk, M., Umezawa, M., and Shaheen, H.M. Ameliorative Role of Cerium Oxide Nanoparticles Against Fipronil Impact on Brain Function, Oxidative Stress, and Apoptotic Cascades in Albino Rats. Frontiers in Neuroscience. 2021; 15: p. e651471. DOI: 10.3389/fnins.2021.651471.

69. Jahani, M., Shokrzadeh, M., Vafaei-Pour, Z., Zamani, E., and Shaki, F. Potential role of cerium oxide nanoparticles for attenuation of diabetic nephropathy by inhibition of oxidative damage. Asian Journal of Animal and Veterinary Advances. 2016; 11: p. 226-34. DOI. http://dx.doi.org/10.3923/ajava.2016.226.234

70. Hamzeh, M., Hosseinimehr, S.J., Karimpour, A., Mohammadi, H.R., Khalatbary, A.R., and Talebpour Amiri, F. Cerium Oxide Nanoparticles Protect Cyclophosphamide-induced Testicular Toxicity in Mice. Int. J. Prev. Med. 2019; 10: p. e5. DOI: 10.4103/ijpvm.IJPVM_184_18.

71. Chen, J., Patil, S., Seal, S., and McGinnis, J.F. Rare earth nanoparticles prevent retinal degeneration induced by intracellular peroxides. Nature nanotechnology. 2006; 1(2): p. 142-50. DOI: 10.1038/nnano.2006.91.

72. Hamad, s. and Hamad, h. Modulation of monosodium glutamate induced histological injuries, histomorphometrical alterations and DNA damage in the mice hepatic and renal tissues by oral administration Nano-cerium oxide and L-arginine and their combination. Egyptian Journal of Histology. 2020; 43(4): p. 1034-1046 DOI: 10.21608/ejh.2020.23155.1244.

73. Hamzeh, M., Amiri, F.T., Beklar, S.Y., and Hosseinimehr, S.J. Nephroprotective effect of cerium oxide nanoparticles on cyclophosphamide-induced nephrotoxicity via anti-apoptotic and antioxidant properties in BALB/c mice. Marmara Pharm J. 2018; 22(2): p. 180-9. DOI. https://doi.org/10.12991/mpj.2018.55

74. Saleh, H., Nassar, A.M.K., Noreldin, A.E., Samak, D., Elshony, N., Wasef, L., Elewa, Y.H.A., Hassan, S.M.A., Saati, A.A., Hetta, H.F., Batiha, G.E., Umezawa, M., Shaheen, H.M., and El-Sayed, Y.S. Chemo-Protective Potential of Cerium Oxide Nanoparticles against Fipronil-Induced Oxidative Stress, Apoptosis, Inflammation and Reproductive Dysfunction in Male White Albino Rats. Molecules. 2020; 25(15): p. e3479. DOI: 10.3390/molecules25153479.

75. Saifi, M.A., Peddakkulappagari, C.S., Ahmad, A., and Godugu, C. Leveraging the Pathophysiological Alterations of Obstructive Nephropathy to Treat Renal Fibrosis by Cerium Oxide Nanoparticles. ACS biomaterials science & engineering. 2020; 6(6): p. 3563-3573. DOI: 10.1021/acsbiomaterials.9b01944.

76. Khorrami, M.B., Sadeghnia, H.R., Pasdar, A., Ghayour-Mobarhan, M., Riahi-Zanjani, B., Hashemzadeh, A., Zare, M., and Darroudi, M. Antioxidant and toxicity studies of biosynthesized cerium oxide nanoparticles in rats. International journal of nanomedicine. 2019; 14: p. 2915. DOI. 10.2147/IJN.S194192

77. Charbgoo, F., Ahmad, M.B., and Darroudi, M. Cerium oxide nanoparticles: green synthesis and biological applications. International journal of nanomedicine. 2017; 12: p. 1401-1413. DOI: 10.2147/ijn.s124855.

78. Qu, S., Dai, C., Guo, H., Wang, C., Hao, Z., Tang, Q., Wang, H., and Zhang, Y. Rutin attenuates vancomycin-induced renal tubular cell apoptosis via suppression of apoptosis, mitochondrial dysfunction, and oxidative stress. Phytotherapy Research. 2019; 33(8): p. 2056-2063. DOI. https://doi.org/10.1002/ptr.6391

79. Talirevic, E. and Jelena, S. Quercetin in the treatment of dyslipidemia. Medical archives. 2012; 66(2): p. 87-8. DOI: 10.5455/medarh.2012.66.87-88.

80. Ren, J., Li, J., Liu, X., Feng, Y., Gui, Y., Yang, J., He, W., and Dai, C. Quercetin Inhibits Fibroblast Activation and Kidney Fibrosis Involving the Suppression of Mammalian Target of Rapamycin and β-catenin Signaling. Scientific Reports. 2016; 6: p. e23968. DOI: 10.1038/srep23968.

81. Moustafa, S, and Ali, M. "The probable protective Effect of Quercetin Against Doxorubicin-Induced Hepatotoxicity in Adult Albino Rats: A Biochemical and Immunohistopathological Study." Ain Shams Journal of Forensic Medicine and Clinical Toxicology 37.2 (2021): 78-97. DOI: 10.21608/ajfm.2021.182110

82. Hashish, F., Abdel-Wahed, M., El-Odemi, M., El-Naidany, S., and Elbatsh, M. Possible protective effects of quercetin on doxorubicin-induced cardiotoxicity in rats. Menoufia Medical Journal. 2021; 34: p. e333. DOI: 10.4103/mmj.mmj_5_20.

83. Widowati, W., Prahastuti, S., Tjokropranoto, R., Onggowidjaja, P., Kusuma, H.S.W., Afifah, E., Arumwardana, S., Maulana, M.A., and Rizal, R. Quercetin prevents chronic kidney disease on mesangial cells model by regulating inflammation, oxidative stress, and TGF-β1/SMADs pathway. PeerJ. 2022; 10: p. e13257. DOI: 10.7717/peerj.13257.

84. Liu, Y., Li, Y., Xu, L., Shi, J., Yu, X., Wang, X., Li, X., Jiang, H., Yang, T., Yin, X., Du, L., and Lu, Q. Quercetin Attenuates Podocyte Apoptosis of Diabetic Nephropathy Through Targeting EGFR Signaling. Frontiers in Pharmacology. 2021; 12: p. e792777. DOI: 10.3389/fphar.2021.792777.

85. Rangan, G.K., Wang, Y., and Harris, D.C.H. Dietary Quercetin Augments Activator Protein-1 and Does Not Reduce Nuclear Factor-κB in the Renal Cortex of Rats with Established Chronic Glomerular Disease. Nephron. 2002; 90(3): p. 313-319. DOI: 10.1159/000049067.

86. Tabatabaeifar, M., Wlodkowski, T., Simic, I., Denc, H., Mollet, G., Weber, S., Moyers, J.J., Brühl, B., Randles, M.J., Lennon, R., Antignac, C., and Schaefer, F. An inducible mouse model of podocin-mutation-related nephrotic syndrome. PloS one. 2017; 12(10): p. e0186574. DOI: 10.1371/journal.pone.0186574.

87. Abd Elbaky, N.A., Hammad, L.N., and Atia, T.A.J.T.E.j.o.h.m. Protective Effect of Simvastatin against adriamycin-induced nepherotoxicity in rats; Biochemical and Histological Study. 2006; 25(1): p. 725-739. DOI. https://dx.doi.org/10.21608/ejhm.2006.17812

الملخص العربى

تأثير جزيئات أكسيد السيريوم متناهية الصغر مقابل كيرسيتين على اعتلال الكلية المحدث بعقار الدوكسروبيسين في ذكور الجرذان البالغة: دراسة بيوكيميائية، نسيجية و كيميائية نسيجية مناعية

شيرين أحمد محمد، ضحى صابر محمد، أسمهان صبري خليفه، سميرة محمود محمد

قسم الهستولوجى، كلية الطب، جامعة سوهج، مصر

المقدمة: يعتبر نموذج الدوكساروبيسين المحدث لاعتلال الكلية نموذج شائع الاستخدام . جزيئات أكسيد السيريوم المتناهية الصغر لها أدوار مضادة للالتهابات ومضادة للأكسدة . كيرسيتين هو نوع من البوليفينول الموجود في المنتجات النباتية المختلفة ويعمل كمضاد للأكسدة.

الهدف من البحث: أجريت الدراسة الحالية لمقارنة التأثير العلاجي المحتمل لجزيئات أكسيد السيريوم متناهية الصغر مقابل كيرسيتين ضد اعتلال الكلية المحدث بعقار الدوكسروبيسين في نقاط زمنية مختلفة.

مواد وطرق البحث: تم تقسيم ٥٥ جرذ بالغ من ذكور الجرذان البيضاء إلى خمس مجموعات. المجموعة الضابطة (المجموعة الأولى). المجموعة الثانية: تم حقن المجموعات المعالجة بـ الدوكسروبيسين داخل الصفاق بجرعة ٢,٥ مجم لكل كجم من الجسم يومًا بعد يوم لمدة أسبوعين ثم توقف عن الحقن ب الدوكسروبيسين لمدة ٣ أسابيع في المجموعة IIa ولمدة ٥ أسابيع في المجموعة IIb. المجموعة الثالثة (مجموعة جزيئات أكسيد السيريوم متناهية الصغر+ الدوكسروبيسين): المحقونة بجزيئات أكسيد السيريوم متناهية الصغر لمدة أسبوعين بعد ٣ أسابيع من إيقاف حقن الدوكسروبيسين في المجموعة IIIa وبعد ٥ أسابيع من إيقاف حقن الدوكسروبيسين في المجموعة IIIb.

المجموعة الرابعة (مجموعة الدوكسروبيسين + كيرسيتين:(المحقونة بـ كيرسيتين لمدة أسبوعين بعد ٣ أسابيع من إيقاف حقن الدوكسروبيسين في المجموعة IVa وبعد ٥ أسابيع من إيقاف حقن الدوكسروبيسين في المجموعة IVb. المجموعة الخامسةV : وقف حقن الدوكسروبيسين لمدة ٧ أسابيع.

أجريت الدراسات البيوكيميائية والميكروسكوبية الضوئية والتركيب الدقيق .كما أجريت الدراسات المورفومترية لنسبة منطقة الكولاجين و صبغة PAS. تم قياس عدد PCNA و WT-١ ونسبة AFP.الايجابية

النتائج: تسبب الدوكسروبيسين في ارتفاع مستويات اليوريا في الدم والكرياتينين ,اتساع التجويف البولى لمحفظة بومان. مع تغيرات تنكسية في الانابيب الكلوية و زيادة في ألياف الكولاجين وقد ظهر ذلك أكثر وضوحا في المجموعة , IIb كان هناك التحام اقدام الخلايا القدمية في التركيب الدقيق . انخفض التعبير الهستوكيميائى المناعى WT-١ فيها بشكل ملحوظ في مجموعة الدوكسروبيسين.مع وزيادة نسبة PCNA وAFP . كان تأثير جزيئات أكسيد السيريوم متناهية الصغر أكثر فعالية مقارنة بالكيرسيتين في تخفيف التغيرات التنكسية الكلوية والتليف مع معالجة إصابة الخلايا القدمية نتيجة الاعتلال الكلوى

الخلاصة: تسبب الدوكسروبيسين في سمية كلوية معتمدة على المدة الزمنية. وكانت جزيئات أكسيد السيريوم متناهية الصغر أكثر فاعلية مقارنة مع الكيرسيتين في تخفيف التغيرات التنكسية الكلوية في نموذج اعتلال الكلية الذي يسببه الدوكسروبيسين.